*Contract n°* ***MAS3-CT97-0090 (DG 12 - ESCY)***

*Title*

# CHARACTERIZATION AND OBSERVATION OF THE SEAFLOOR WITH A NEW MULTI-BEAM FRONT-SCAN SONAR SYSTEM

*Acronym*

## COSMOS

# *Final report*

***Tasks 4.1*** *- Data Alignment - Imaging*

***Tasks 4.2*** *- Interferometry - Bathymetry*


**UNIVERSITÉ PIERRE ET MARIE CURIE**
**LABORATOIRE DE MÉCANIQUE PHYSIQUE**
**(CNRS UPRESA 7068)**

*Redactor : Pierre Cervenka*

# CONTENT

# ANNEXES

# INTRODUCTION

The technical annex of the contract referenced the following reports with regard to Task 4 (Bathymetry and Imaging) :

- R4.1.1 Methods and SW for data conversion (Task 4.1)
- R4.1.2 Imaging and Bathymetry (Tasks 4.1 and 4.3)
- R4.2 Interferometric process (Task 4.2)

LMP-UPMC and DIBE addressed several different specific issues within Task 4. Hence, it has been found more convenient to compile two separate reports. The present text gathers the only contribution of LMP-UPMC :

- Section 1 covers Task 4.1 (Data Alignment - Imaging), so that it encompasses the planed report R4.1.1 and part of R4.1.2.
- Section 2 covers Task 4.2, and is equivalent to the planed report R4.2 and part of R4.1.2.

A four days survey has been performed in the surroundings of Barcelona (22 October – 3 November 1999) on board the catamaran l'*Europe* that is operated by IFREMER. The survey routes were prepared by ICM-CSIC. The selected areas presented a large variety of nature and relief, with several remarkable targets. About 81 000 pings have been recorded (100 GBytes archived). It provides a large database for developing and testing innovative processes in the fields of imagery and bathymetry.

More specifically, redundancy of information afforded by the footprint overlap between successive pings allows to take advantage of the imaging compound technique. In addition, the interferometric capability yields a powerful tool for locating properly the spatial origin of incoming echoes. This report addresses the main issues related to the development of the new processing tools.

The COSMOS system records both base-banded signals received by each elementary transducer (raw data), and in-line beam-formed data. The latter are only used to build a control image during acquisition. The technical description of the acquisition setup is in the final report on Task 2.

The architecture of the files involved in the post-processing is described in Annex 4 of the final report on Task 2 (Section 3.4.4 – “Format of post-processed data”). The first step of the processing consists of building calibrated, compressed beamformed data. Other types of information (navigation and attitude) are synchronized and merged to the acoustical data. The new files are processed to build backscatter images and to produce bathymetry. Section 1 addresses the preliminary step (beamforming, synchronization) and the imaging application. Section 2 is devoted to the bathymetry application. In addition, several specific technical and theoretical matters are gathered in Annexes.

# 1. BEAMFORMING – NAVIGATION – ATTITUDE – IMAGING

## 1.1 DESCRIPTION OF TASK 4.1

### 1.1.1 Objectives

This task concerns the following items :

- Time-space correspondence between data acquired during successive pings (common reference system) ;
- Production of gridded individual images (map projection of backscatter echoes) ;
- Fusion of these individual images (mosaic).

### 1.1.2 Achievements

- Deliverable #1 : Methods and software for data alignment/conversion.

  All recorded data – raw acoustic data, navigation and attitude – have been properly synchronized at a post-processing stage. Beamformed data have been built by taking into account the corrections derived from the calibration of the system. Positioning information is computed and appended to the file (ping basis format).

- Deliverable #2 : Methods and software for production of images.

  An interpolation scheme has been set up to grid the data. A specific weighting is applied in order to balance the contribution of the different points of view. A mapping management allowed to process large areas

- Deliverable #3 : Images.

  Image enhancement (adjustment of mean level, contrast enhancement) is finally performed. All four covered zones have been processed. The resulting images have been delivered to partners for evaluation (Task 6.1).

## 1.2 BEAMFORMED DATA

### 1.2.1 Data structure

Raw transducer data undergo several compensations and transforms in order to build the beamformed data that are needed for subsequent studies on characterization, imaging and bathymetry. This section addresses the building of the types of blocks thereafter called “Acou_block” (Figure 1.1) and “Phas_block” (Figure 1.2). The data blocks included in standard post-processed files (i.e. File block + Ping block + Data blocks) are such blocks. For instance, files tagged with the suffix “.acu” contain the single type of blocks “Acou_block”.

```
typedef struct {
  def_packet_id packet_id; // sizeofpacket = sizeof(def_acou_hd) + depends on number of bases, i.e.
                           //          + (0 or 1 ) * acou_hd.nb_tixels*sizeof(char)
                           //          + (0 or 1 or 2) * acou_hd.nb_beams*acou_hd.nb_tixels*sizeof(char)
                           //          + (0 or 1) * acou_hd.nb_beams*acou_hd.nb_tixels*sizeof(short)
                           // typeofpacket = Acou_pk
  long  status;            //(status & (1L<<base_0_stb)) -> base_0, (status & (1L<<base_1_stb)) -> base_1
  short nb_beams;          // default : 31
  short nb_tixels;
  short aperture;          // 1/100 deg. (default 2500)
  short noise_threshold;   // dB  (default=-32000, meaning undefined)
  short noise_index;       // default : nb_tixels
  short depth_threshold;   // dB  (default=-32000, meaning undefined)
  short depth_index;       // default : 0 (if < 0, abs(depth_index) is questionable)
  short source_level;      // in .1 dB rms ref. 1µPa @ 1m  (default : 2072)
  short sensibility;       // in .1 dB (system_unit / µPa)   (default : -915)
  short dynamic;           // dB                             (default : 64)
} def_acou_hd;

//  Acou_block {           // For info only. This is NOT a C structure
//  def_acou_hd   acou_hd;
//  short         max_level[acou_hd.nb_tixels]; // in dB
//  unsigned char  beams_base0[acou_hd.nb_beams][acou_hd.nb_tixels];// if(ac_hd.status&(1L<<Base_0_stb))
//  unsigned char  beams_base1[acou_hd.nb_beams][acou_hd.nb_tixels];// if(ac_hd.status&(1L<<Base_1_stb))
//  }
```

Figure 1.1 : Structure of blocks concerning backscatter strength

```
typedef struct {
  def_packet_id packet_id; // sizeofpacket = sizeof(def_phas_hd)
                           //                + angle_hd.nb_beams*angle_hd.nb_tixels*sizeof(short)
                           // typeofpacket = Phas_pk
  long  status;
  short nb_beams;          // default : 31
  short nb_tixels;
} def_phas_hd;

//  Phas_block {           // For info only. This is NOT a C structure
//    def_phas_hd  phas_hd;
//    short        phase[phas_hd.nb_beams][phas_hd.nb_tixels];  // unit : 1e-4*rad.
//  }
```

Figure 1.2 : Structure of blocks concerning the interferometric phases

The recorded signals are organized in 2-D arrays : One dimension is the elementary transducer index ; the second dimension is time. Accordingly, the processing of each ping is split into two successive stages. Temporal sequences are handled in the first stage ; The second stage deals with data along the other dimension, i.e. in relation to the beam directions.

### 1.2.2 Time processing

The time processing includes :

- Offset removal (high pass filtering)
- Compensation for the elementary transducers response

  The uneven sensitivity of the receiving arrays elements, as well as the dispersion of the phase responses are compensated in the beamforming process. This compensation is based on the calibration that is described in the Final Report on Task 2 (Section 1 – Antennae – Figures 1.16 and 1.17).
- Time varying gain removal

  The varying gain that was applied in-line, during acquisition, is removed.
- Pulse compression

  The transmitted signal is Linearly Frequency Modulated. The complete parameters are given in Annex 5.1. At receive, the electronics hardware performs a base-band demodulation, and digitizes the resulting complex signals (Annex 4.1). Pulse compression is achieved by means of a correlation with the replica of the base-banded digitized transmitted signal. The replica is normalized so as to compensate for the processing gain caused by the compression.
- Tapering of the antenna elements and range focusing

  Complex multiplicative coefficients are applied. They depend on the index of the sequence that is considered, i.e. the abscissa $x_i$ of the transducer element (the origin being centered), and on the position in the sequence, i.e. the range $r$. Each factor corresponds to the combination of : 1) a taper coefficient that performs a shadowing of the array in order to reduce the side lobe levels ; 2) the quadratic phases that account for the wave front curvature needed to focus at range $r$ (Fresnel approximation) :

$$a(x_i, r) = \exp\left( \ln(u) \frac{x_i^2}{(l/2)^2} \right) \exp\left( jp \frac{x_i^2}{l_0 r} \right) \tag{1.1}$$

  The weighting factor for the end elements of the array is equal to $|a(\pm l/2, r)| = u = 0.2$ ; $l$ denotes the length of the antenna. Note that focusing is actually a matter of time delays. The equivalence with a phase shift as expressed with the second term in (1.1) is justified in Annex 4 : $l_0$ is the wavelength corresponding to the central frequency of the chirp signal (100 kHz).

### 1.2.3 Space processing

The transformed 2-D array is then processed along the other dimension :

- Beamforming

  31 beams (per receiving array) are formed in the equispaced directions $q_j$ within a sector that is 25° wide in azimuth. The corresponding complex coefficients are :

$$b(x_i, q_j) = \exp\left(jk_0 x_i \sin q_j\right) \quad \text{with} \quad k_0 = 2p/l_0 = w_0/c\,. \tag{1.2}$$

  Hence, the result takes the form of two complex 2-D arrays $s_{1;2}(t, q_j)$.

- Standard compensation for losses

  The amplitude of echoes received from range $r$ are partially compensated for losses that are evaluated according to the backscattering regime. Expressed in terms of intensity, the one-way propagation losses caused by geometrical spreading and attenuation (coefficient α) are given by :

$$A_{\text{one-way}} = \left(e^{-ar}/r\right)^2 \tag{1.3}$$

  These losses are partially compensated by the size of the insonified footprint that increases with range :

$$S_{\text{footprint}} = rq_b \frac{L/2}{\sin x}\,, \tag{1.4}$$

  where $q_b$ is the width in azimuth of a single beam, $x$ is the incident angle on the seafloor, and $L$ is the equivalent propagation length of the pulse compressed signal (about 40 cm). The net effect for backscattered echoes is given by the decreasing law :

$$A_{\text{echo}} = A^2_{\text{one-way}} S_{\text{footprint}} = \frac{\exp\left(-4ar\right)}{r^3} \frac{q_b\, L/2}{\sin x} \tag{1.5}$$

  The relief is not known at this level of the processing. Consequently, the time evolution of the incidence angle is not known either. In addition, the exact definitions of the beam width ($q_b$) and the signal duration ($L/c$) are rather lousy. Our concern is to transform data in such a way that subsequent users can easily master and retrieve the level compensations. Hence, the applied multiplicative factor $f_a$ that is actually applied (in terms of amplitudes) is based on the only part in (1.5) that depends on range :

$$f_a(r) = r^{3/2} \exp\left(2ar\right) \tag{1.6}$$

  Hence, ***an additional correction must be added to the values stored in Acou_blocks in order to estimate the backscattering strength per unit of surface as a function of the incidence angle :***

$$\boxed{\text{Correction} = -10\log\left(q_b L/2\right) \approx +22\ \text{dB}} \tag{1.7}$$

  with $q_b \approx 1.5°$ and L/2 ≈ 25 cm

- <u>Coding</u>

  The analog to digital conversion is performed by the electronics hardware over 12 bits. Such a relatively small dynamic can be used because a time varying gain is applied with the front-end amplification. Integer data are converted into type "double" at the very beginning of the post-processing stage. Then, the amplitude of beamformed echoes is organized in 2D arrays whose dimension is $nb\_beams \times nb\_times$. Each column corresponds to one beam ; each row corresponds to a time sample.

  For each ping, a vector **max_level**[*nb_times*] is built and archived. Each element of this vector records the maximal level of the corresponding row in the 2D-array. Hence, the elements of a given row can be coded in a log scale that is referenced to this maximal value. The type of the resulting arrays **beam_base**x[*nb_beams*][*nb_times*] is "unsigned character", which provides 256 levels. The coding is performed over a fixed dynamic range (dynamic = 64 dB). This range is considered to be sufficient to account for the physical variations of the backscattering strength observed at a constant range of a given ping. The effect of quantization is negligible (dynamic / 64 = 0.25 dB), and the space saving is significant.

  But for the correction (1.7) and the directivity of the antennae, the values stored in **beam_base**x[] are equivalent to surface backscatter indexes. This is because the elements of vector **max_level** are also offset before recording to take into account the source level and the sensitivity of the receiving antenna. The calibration of the transmitter yielded :

  $$SV = 151 \text{ dB ref. } 1\mu\text{Pa @ 1m / V},$$

  The antenna is fed with 1290 $V_{pp}$, i.e. the peak amplitude 645 $V_p$. The source level (referred to peak amplitude) can be then estimated with :

  $$SL_p = SV + 20 \log10(v_p) \approx 207.2 \text{ dB ref. } 1\mu\text{Pa}_{\text{peak}} \text{ @ 1m}$$

  The sensitivity of the receiving arrays is expressed in terms of numerical unit, as recorded, per unit of pressure :

  $$SH = -91.5 \text{ dB (ref. 1 bit / } \mu\text{Pa)}$$

  Note that PC1 records 16-bits words. The 12-bits data delivered by the analog-to-digital converters take place at the most significant bits of these words. A numerical unit refers here to the word's least significant bit (0Bxxxxxxxxxxxx0001).

  Borrowing to the C idiom, the performed correction takes the form :

  $$\text{max\_level} -= SL_p + SH.$$

- <u>Noise</u>

  The mean effect of the standard range varying gain described at the beginning of this section is to equalize the magnitude of the data, as far as they account actually for the amplitude of the backscattered echoes, i.e. the signal to noise ratio (SNR) is high. Within a rough model which is quite sufficient here, it can be assumed that the noise level does not depend on range. At far range, the signal level decreases dramatically. When the SNR is low,

the standard range varying gain applied at post-processing boosts the noise level which therefore grows exponentially. This behavior is depicted in Figure 1.3. A simplified algorithm has been set up to estimate the maximal useful range beyond which the SNR is too low to derive reliable information for imaging or bathymetry.

Part of the sequence **max_level**[] is used to compute the mean backscatter surface strength ($s^2$) over the first half portion of the whole recorded range.

A mean value ($n^2$) that is proportional to the noise level is then estimated over a small portion of the record, at the end of the ping. This calculus is made with the last elements of **max_level**[], but removing the compensation for losses, $f_a(r)$, given in (1.6). This technique relies indeed on the fact that $f_a(r_{\max})\, n^2 > s^2$. The searched range $r_{\text{noise}}$ is the intersection of the curve $f_a(r)\, n^2$ with the mean value $s^2$ (respectively the red curve and the green horizontal line in Figure 1.3).

With the above notations, it must be remembered that $n^2$ is homogeneous to a backscatter strength index. An estimate of the noise level is computed by adding the source level, and introducing a compensation related to the pulse compression processing gain.

$$\text{noise\_threshold} \equiv n^2_{\text{dB}} + \text{SL}_\text{p} + \textit{compression\_snr}$$

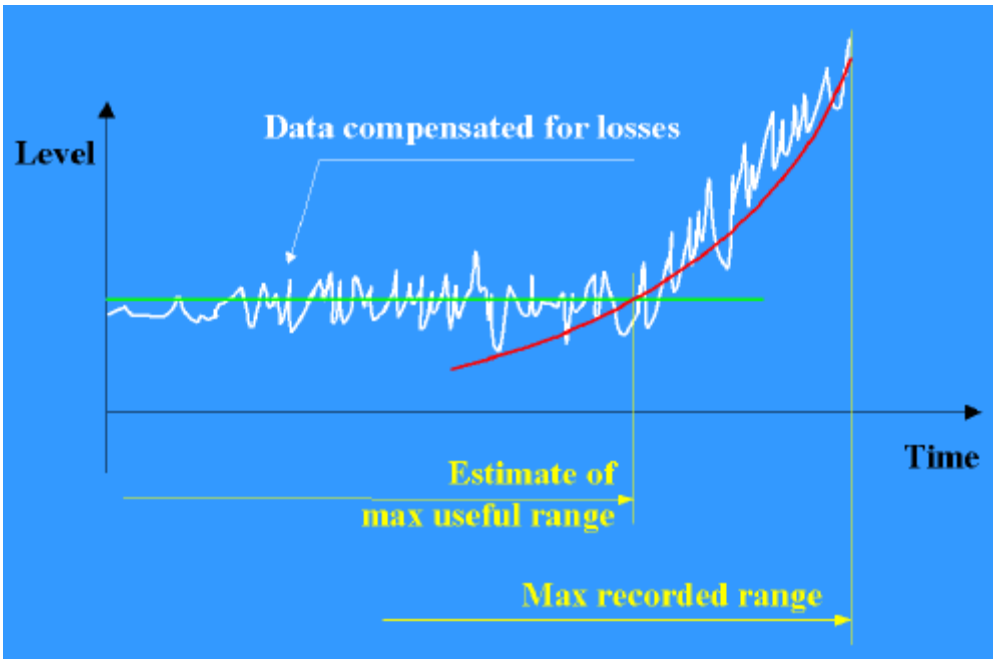


Figure 1.3 : Detection of low signal to noise ratio

- Phase

The differential phases $j(t, q_j) = \arg(s_1 s_2^*)$ are stored in 2-D arrays that build the "Phas_block" described in Figure 1.2. Phases are here defined in the domain $]-\pi, \pi]$.

## 1.3 SHIP POSITION AND ATTITUDE –SYNCHRONIZATION

### 1.3.1 Principle of operation

The parameters that are recorded by PC2 are : (see Final Report on Task 2 – Section 3 – "Data links and storage, system controls and displays").

- Clock giving the absolute current date
- GPS position, i.e. latitude and longitude
- True heading, i.e. referenced to the geographical North
- Attitude, i.e. pitch, roll and heave
- Synchronization message from the sonar (start of ping transmit)

The incoming rate of the clock is 1s ; it is about 2s for navigation packets ; the order of magnitude is in the tens of ms for attitude data ; the ping interval may vary between a few tenths of second up to several seconds. The sampling of these parameters cannot indeed be considered as perfectly regular, nor synchronized. A time tag derived from a common high precision counter (PC2) is appended to each collected message. This tag allows to perform the required synchronization.

The implementation of the post-synchronization follows a classical scheme : while the records are read sequentially, the parameters are sorted by type, and fill specific buffers. During the process, data that are no longer needed are discarded from the buffers.

The output of this synchronization task consists of standard post-processed files (i.e. File block + Ping block + Data blocks) that are tagged with the suffix ".nav". They contain the single type of data blocks named "Ship_block", that is described thereafter. The post-synchronization of the whole Barcelona survey lasts a few minutes (Pentium II 350 MHz). Other types of files can be then created. For instance, the ".bms" files collect "Ship_block", "Acou_block" and "Phas_block" types of blocks. Note that the size of the created files is purposely limited (< 30 MB). The beginning and the end of a survey line dictate also file caesuras (detection of a gap in the recording larger than 10 s).

### 1.3.2 Position and attitude data blocks

This section addresses the building of the type of blocks named "Ship_block" (Figure 1.4). This type is designed to carry the collected information that is not acoustics. We focus here on the navigation and the attitude of the ship. The format of the input data (i.e. files written during sonar acquisition) are described in Annex 3 of the final report on Task 2 ("format of attitude and navigation files"). The new blocks are built on a ping by ping basis, i.e. the origin of time for each block is the start of ping transmit. A block consists of a header that is followed by an array of data.

A single set of date, position and heading is computed for each ping, at the time origin, and is written in the header. Because the information that the date message carries is perfectly synchronized with the associated time tag, both be-

ing indeed linear with time, the date of ping transmit is obtained by a mere linear interpolation. Position and heading are derived by a least square fitting (second degree). The fitting uses the incoming data whose time tag belongs to a temporal window that is centered on the required instant. The window is tapered by a truncated Gaussian envelope (20% at ends). The size of the window is 6 s to interpolate the heading. The width is much larger to compute the position (20 s). Such a size is needed to reduce a digitization effect of the GPS messages : the least significant digit in the coding of latitude and longitude represents thousandths of minutes, i.e. 1 m or so. This increment is indeed too large with respect to the radial resolution of the sonar (about 30 cm), and is also the same order of magnitude as the distance that the ship runs between successive pings.

```
typedef struct {
  def_packet_id packet_id; // sizeofpacket = sizeof(def_ship_hd)
                           //                + nb_ship_att*sizeof(def_ship_att)
                           // typeofpacket = Ship_pk
  long  status;            // (1L << Leg_begin_stb) -> start, (1L << Leg_end_stb) -> end
  char  string[32];        // possibly bathycelerimetry name
  long  longitude;         // 1.e7 * longitude (in decimal degrees) (W <0, E >0)
  long  latitude;          // 1.e7 * latitude (in decimal degrees)  (S <0, N >0)
  long  offset_heading;    // 1/100 deg. (default : 0)
  long  heading;           // 1/100 deg.
  short v_x;               // speed in mm/s (> 0 towards East)
  short v_y;               // speed in mm/s (> 0 towards North)
  short temperature;
  short salinity;
  short offset_pitch;      // 1/100 deg.
  short offset_roll;       // 1/100 deg.
  short decim_att;         // one ship_att (attitude) data every other decim_att tixels
  short nb_ship_att;       // number of ship_att (attitude) data
} def_ship_hd;

typedef struct {
  short pitch;             // 1/100 deg.
  short roll;              // 1/100 deg.
  short heave;             // mm
} def_ship_att;

//  Ship_block {           // For info only. This is NOT a C structure
//    def_ship_hd  ship_hd;
//    def_ship_att ship_att[ship_hd.nb_ship_att];
//  }
```

Figure 1.4 : Structure of blocks concerning navigation and attitude data

The sampling rate of the acoustic data is 4 kHz (exactly 256 µs). Such a high rate is not needed to describe the evolution in attitude because the corresponding spectral contents are significant only at much lower frequencies. Hence, the sampling rate is decimated to build the attitude records. The chosen factor (decim_att = 64) yields a period of 16 ms, i.e. the same order of magnitude as the original sampling of the attitude parameters as delivered by the Vertical Reference Unit. The re-sampling is performed by linear interpolation of the nearest available data that surround the required instant in the incoming stream. The number of element of the resulting array is dictated by the delay $\Delta t$ between successive pings, namely nb_ship_att = min{64, $\Delta t$ / 16 ms}.

## 1.4 DATA POSITION FOR IMAGING

### 1.4.1 Organization

Mosaic images of the backscattered echoes are built in three steps :

1) Attitude and navigation data, organized on a ping basis ("Ship_block"), are processed to derive the relative horizontal location of the beamformed data. This step outputs blocks of type "Coor_block" (Figure 1.5).
2) Backscatter indexes are interpolated and stacked on grids to build multi-layer mosaic structures.
3) The multi-layer mosaics are merged to make images.

```
typedef struct {
  def_packet_id packet_id; // sizeofpacket = sizeof(def_coor_hd)
                           //                + coor_hd.nb_beams*sizeof(short)
                           //                + sum_on_beams(coor_hd.nb_coor[beam])*sizeof(def_coor)
                           // typeofpacket = Coor_pk
  long  status;
  long  longitude;         // 1.e7 * longitude (in decimal degrees)  (W < 0,  E > 0)
  long  latitude;          // 1.e7 * latitude    (in decimal degrees)  (S < 0,   N > 0)
  short x_unit;            // mm
  short y_unit;            // mm
  short z_unit;            // mm
  short z_ref;             // Used for flat bottom projection :
                           // (in z_unit) z_ref=-1 automatic depth search
                           //             z_ref=0  slant range projection
                           //             z_ref>0  a priori flat bottom_depth
  short nb_beams;          // default 31
} def_coor_hd;

typedef struct {
  short x;                 // in x_unit
  short y;                 // in y_unit
  short z;                 // in z_unit
  short a;                 // 1.e-4 rad. (grazing angle)
  unsigned char q;         // quality factor (on z)
  short index;             // corresponding acoustic tixel
} def_coor;

//  Coor_block {           // For info only. This is NOT a C structure
//    def_coor_hd  coor_hd;
//    short        nb_coor[coor_hd.nb_beams];
//    def_coor     coor[nb_coor[beam0] + nb_coor[beam1] + …)];
//  }
```

Figure 1.5 : Structure of blocks concerning data positioning

This section addresses the first step. An estimated location of the origin of the incoming echoes must be associated to each acoustic data. The local flat bottom assumption is used. This approximation is common in backscatter imaging : it does not introduce any noticeable distortion as far as the relief is smooth enough. The refraction is neglected as the implied corrections would be still smaller than the error caused by the previous approximation. The horizontal translation of the ship during a single ping is not taken into account either.

We studied thoroughly the effect of the platform translation between ping transmit and echoes receive. Simple but accurate formulas have been derived ; preliminary results were given in the report on progress in Task 4.2. However, the orders of magnitude involved in this issue are not relevant with COSMOS : An upper bound of the error is half the distance that is run during receive of echoes, i.e. less than 40 cm with an usual max range of 300 m and a ship speed of 3 knots.

A reference altitude of the antennae is estimated for each ping. Then, heading, attitude data, beam steering angles, depth and ranges are used to derive the searched locations in the local horizontal planes.

### 1.4.2 Analytical solution

Notations, coordinate systems and rotation matrices are described in Annex 1 ("Data positioning"). In the flat bottom assumption, the problem consists of finding the horizontal location of a point **M** in the FCS, given the depth *z*, the slant range *s*, and the beam angle *b*. Point **M** verifies the relation :

$$\mathbf{a}_y.\mathbf{M} = s\sin b \ , \quad \text{with} \quad s = \sqrt{x^2 + y^2 + z^2} \ , \quad \mathbf{M}_{FCS} = \begin{bmatrix} x \\ y \\ z \end{bmatrix} \quad \text{and} \quad \mathbf{a}_{y_{FCS}} = \mathbf{T}_0\mathbf{T}_1\mathbf{T}_2 \begin{bmatrix} 0 \\ 1 \\ 0 \end{bmatrix} \tag{1.8}$$

Solving (1.8), one finds that the horizontal mapping of **M** in the FCS reads :

$$\boxed{\begin{bmatrix} x \\ y \end{bmatrix} = \begin{bmatrix} \cos(h+d) & -\sin(h+d) \\ \sin(h+d) & \cos(h+d) \end{bmatrix} \begin{bmatrix} \sqrt{s^2 - z^2 - v_0^2} \\ v_0 \end{bmatrix}} \tag{1.9}$$

$$\begin{bmatrix} \sin d \\ \cos d \end{bmatrix} = \frac{1}{\sqrt{1-(\sin l \sin p + \cos l \sin r)^2}} \begin{bmatrix} \sin l \cos p - \cos l \sin r \tan p \\ \dfrac{\cos l}{\cos p}\sqrt{1-\sin^2 p - \sin^2 r} \end{bmatrix}, \tag{1.10}$$

$$v_0 = \frac{s\sin b - z\sin a}{\cos a} \tag{1.11}$$

$$\sin a = \cos l \sin r + \sin l \sin p \ , \tag{1.12}$$

The solution given by (1.9) applies whatever is the mounting angle *l*. However, useful approximations can be derived in practical implementations, i.e. for front-looking and sidescan sonars. In the former case (COSMOS), *l* is close to zero. Eq. (1.10) reads :

$$d = \arctan \frac{\tan l \cos^2 p - \sin r \sin p}{\sqrt{1-\sin^2 p - \sin^2 r}} \ , \tag{1.13}$$

so that the approximation $d \approx l - rp$ always holds. In addition, the replacement of *a* by *r* in evaluating $v_0$ with (1.11) can be investigated, depending on the required accuracy.

With a side-scan system, Eq. (1.10) reads :

$$d = \frac{p}{2} + \arctan \frac{\sin l' \sqrt{1 - \sin^2 p - \sin^2 r}}{\cos l' \cos^2 p + \sin l' \sin r \sin p} \quad \text{with} \quad l' = l - \frac{p}{2} \tag{1.14}$$

Because $l'$ is close to zero, the approximation $d \approx l$ applies. The approximation $a \approx p$ can be also investigated to evaluate $v_0$, depending on the required accuracy.

<u>Summary</u>

- With a forward looking geometry the horizontal location of the target is given by :

$$\boxed{\begin{bmatrix} x \\ y \end{bmatrix} = \begin{bmatrix} \cos h & -\sin h \\ \sin h & \cos h \end{bmatrix} \begin{bmatrix} \sqrt{s^2 - z^2 - v_0^2} \\ v_0 \end{bmatrix}} \quad \text{with} \quad \boxed{h = h + l - rp} \tag{1.15}$$

  where $v_0$ is given by (1.11) that is computed either exactly with (1.12) or approximately with $a = r$.

- With a sidescan system, the following alternative of (1.9) yields a better presentation of the result :

$$\boxed{\begin{bmatrix} x \\ y \end{bmatrix} \approx \begin{bmatrix} \cos h & -\sin h \\ \sin h & \cos h \end{bmatrix} \begin{bmatrix} -v_0 \\ \sqrt{s^2 - z^2 - v_0^2} \end{bmatrix}} \quad \text{with} \quad \boxed{h = h + l'} \tag{1.16}$$

  where $v_0$ is still given by (1.11) that is computed either exactly with (1.12) or approximately with $a = p$.

<u>Note</u> : In both cases (forward and side looking geometry), the approximations are derived by using developments up to the second order. The approximations for $h$ given in (1.15) and (1.16) must be used in the numerical implementation of the rotation matrix. They are justified because roll and pitch are small angles, whereas $l$ and $l'$ are **very** small compared to unit.

It can be also noticed that roll and pitch are permuted in the proposed approximation of $a$, when switching from the forward to the side looking configuration. This symmetry does not hold in the expression of $d$ : Roll and pitch appears in the forward looking configuration. The reason is that the axis $\mathbf{s_x}$ and $\mathbf{s_y}$ are not equivalent with respect to the heading : $\mathbf{s_x}$ belongs always to the vertical plane that gives the heading, whereas the vertical plane that contains $\mathbf{s_y}$ is generally not exactly perpendicular to the former.

### 1.4.3 Implementation

The first bottom return is searched by analyzing the sequence **max_level**[]. The algorithm tracks the bottom profile between successive pings so as to avoid false responses caused by fish schools. The results are recorded in “acou_block” and “Coor_block“ headers (depth_index is a number of time samples, and z_ref is scaled by z_unit).

Eqs. (1.11) (1.12) and (1.15) are used. The origin of coordinates is the vertical projection of the GPS antenna at ping transmit. Consequently, a lever compensation is added for taking into account the horizontal location of the COSMOS module relatively to the GPS antenna : Both units lie in the same alongtrack plane, but the GPS antenna is 5.1 m closer to the bow than the COSMOS antennae.

The x_ and y_ axis of the Cartesian system used in the C codes point respectively to East and North (Note that they correspond respectively to the vector $\mathbf{f_y}$ and $\mathbf{f_x}$ defined in Annex 1.2). The scales, x_unit and y_unit, are given in the “Coor_block“ header. Acoustic data are organized in 2-D beam × time structures. Positions are stored as elements of the “**coor**” arrays which are also sorted by beam. However, the constant, high temporal sampling rate of acoustic data is not kept. With increasing ranges, the curvature of the beam footprints vanishes, and horizontal range tends to be linear with slant range. Consequently, the distance between positions to be linearly interpolated can increase with range. Practically, each beam is assigned nb_coor[beam_index] positions . Within each beam, the sampling decreases linearly with range ; The actual correspondence between each individual position and the acoustic samples is given by beams_basex[][coor[].index].

Given the flat bottom assumption, each position can be also completed with a grazing angle. In addition, latitude and longitude of each ping is duplicated from “Ship_block” to “Coor_block” headers so that the former type of blocks is no longer needed. Consequently, “.bms” files are transformed into “.abc” files that collect the only “Acou_block” and “Coor_block” types of blocks.

A statistical analysis of the dependence in azimuth and site of the backscatter strengths is described in Section 1.5 of the final report in Task 2. This analysis has been performed with “.abc” files because acoustic data can be properly referenced (beam index and grazing angle). Once the calibration is obtained, a compensation is introduced in data of the “Acou_block” blocks to form a new set of “.abc” files. The correction is purposely limited to the normalized response in azimuth which accounts mainly for the transmitter beam pattern : It is mandatory to avoid any significant change in the response in site in order to enable studies about seafloor characterization.

### 1.5 INTERPOLATION AND MAPPING

The map management and interpolation process are presented in Annex 3. We built images with a pixel size equal to 50 cm. It is larger than the radial resolution of the sonar (about $L_r$ =30 cm), but still consistent with its angular resolution (about $q_b$ = 1.5°, i.e. 50 cm at a range of 20 m).

The size of the physical resolution cell varies with the incidence angle. The surface $S_c$ of the cell is the product of the azimuth and radial resolutions, respectively $d_a$ and $d_r$. Given the distance $h$ between the antenna and the sea floor, the evolution of $S_c$ with the incidence angle $x$ is :

$$d_a = rq_b = \frac{hq_b}{\cos x} \quad \text{and} \quad d_r = \frac{L_r}{\sin x} \quad \Rightarrow \quad S_c(x) = d_a d_r = \frac{2hL_r q_b}{\sin(2x)}, \tag{1.17}$$

so that $S_c$ is minimal at $\xi$ = 45°. It seems reasonable to emphasize the information corresponding to the finer resolution. Therefore, a weighting factor is introduced in the mapping process. This factor lowers also the contribution of the outer beams.

The following elements are finally mapped in the ping space P (see Annex 3) :

- $w$ weight factor
- $wi$ tapered intensity of echoes
- $x$ incidence angle

Then, the mapped ping is stacked in the active window S of the survey space. The S space consists of 32 mosaic layers. Each layer corresponds to a small range of incidence angle, and is made of two elements ($W$=Σ$w$, $I_w$=Σ$wi$). The element $x$ in the P space dictates towards which layer in S the associated elements ($w$, $wi$) must be dispatched.

Once a complete survey is processed, a multi-layer mosaic is available. Such a structure is well suited to study seafloor characterization. However, we address here the only imaging application. For this purpose, echoes from different incidence angles are merged. Consequently, it is mandatory to balance properly their relative intensities. We based the compensation on the statistical dependence in site described in Section 1.5 of the final report in Task 2. Note that if the mosaic is only intended for imaging purpose, the correction can take place at an earlier stage of the process, e.g. while mapping the data in the P space.

Depending on the required range of incidence angles, several layers are merged to build a single layer with two elements ($\boldsymbol{W}$=Σ$W$, $\boldsymbol{I_w}$=Σ$I_w$). A map that is homogeneous to mean backscatter indexes is derived by doing the ratio of these elements : $I = \boldsymbol{I_w} / \boldsymbol{W}$. (a null weight means indeed that no data is available for that pixel). A bitmap representation is finally elaborated. Scaling and image enhancement are addressed in the next section : Note that all the involved histograms are actually adapted so as to take into account the weight factors $\boldsymbol{W}$ ; The implemented formulae are not displayed to keep the presentation clearer.

## 1.6 IMAGE ENHANCEMENT

### 1.6.1 Notations

The purpose of the processes described here is to adjust the colormap of a picture so as to improve the amount of information that is perceptible by a viewer. Two basic transforms are investigated and merged : median gray level shift, and histogram equalization.

One uses the following conventions :

- the scale of gray levels is normalized, i.e. $g \in [0, 1]$
- this scale is quantized with the pitch $\Delta g << 1$.
- Although not mathematically rigorous, the continuous notation is conveniently used instead of the discrete representation. The gray level histogram of an image is considered here as a pseudo-continuous function $H(g)$, such that $\int_0^1 H(g)dg = N$, where $N$ is the number of pixels that carry information. The actual histogram is only defined on discrete bins, $\hat{H}(g_i)$, the relation with the continuous representation being $\hat{H}(g_i) = \int_{g_i-\frac{1}{2}\Delta g}^{g_i+\frac{1}{2}\Delta g} H(u)du$. The normalized histogram is denoted $h(g) = H(g)/N$.

### 1.6.2 Median

The median gray level $g_m$ is defined by :

$$\int_0^{g_m} h(g)\mathrm{d}g = .5 . \tag{1.18}$$

Given $e_a$, $e_b << 1$, let us define the lower and upper limits $g_a$ and $g_b$ with :

$$\int_0^{g_a} h(g)\mathrm{d}g = e_a , \quad \int_{g_b}^{1} h(g)\mathrm{d}g = e_b . \tag{1.19}$$

Hence, there is necessarily : $0 \le g_a < g_m < g_a \le 1$.

Let us define a targeted median level $q_m$ ($0 < q_m < 1$, usually, $q_m = .5$ is required). A simple monotonous transform that maps $g_a$, $g_m$ and $g_b$ into 0, $q_m$ and 1, respectively, is defined with :

$$\begin{aligned} &q(g_a \le g \le g_b) = \frac{g-g_a}{g_b-g_m}\left(\frac{g-g_m}{g_b-g_a} + q_m\frac{g_b-g}{g_m-g_a}\right), \\ &q(0 \le g \le g_a) = 0, \\ &q(g_b \le g \le 1) = 1. \end{aligned} \tag{1.20}$$

### 1.6.3 Equalization

Histogram equalization is obtained with the gray level transform :

$$g'(g) = \int_0^g h(u)\mathrm{d}u\,, \tag{1.21}$$

The histogram of a so transformed image is flat. Whenever the original image is made of large homogeneous regions with different average gray levels, this global process may still keep hidden the subtle but meaningful variations of intensity that occur within each region.

To overcome this problem, each region $A$ can be processed with a modified transform in which the integrand, $h(u)$, in (1.21) is replaced by a reference function, $\gamma_A(u)$, that takes into account the local histogram $h_A$ evaluated around $A$ :

$$g'_A(g) = \int_0^g g_A(u)\mathrm{d}u \quad \text{with} \quad g_A(g) = (1-b)\,h(g) + b\,h_A(g) \tag{1.22}$$

With $b = 1$, the equalization is strictly local : the details of each region are strongly emphasized, but the relative mean levels between these regions are completely lost. At the opposite, $b = 0$ gives back (1.21) with its drawback. Hence, the coefficient $b$ allows to balance properly the visibility of the information at both the small and large scales.

From a practical point of view, each local histogram $h_A(u)$ is the weighted sum of elementary histograms $H_i$ computed over small adjacent square domains :

$$h_A(g) = \frac{\sum w_i^{(A)} H_i(g)}{\sum w_i^{(A)} N_i} \tag{1.23}$$

($N_i$ denotes the number of samples used to build each elementary histogram).

A complete histogram equalization throw away definitively an interesting information : the histogram itself ! Actually, this is generally not suitable to remove it all from the pictorial representation. A convenient arrangement is to tune (1.22) by using a coefficient $a$ :

$$g'(g) = (1-a)\,g + a\int_0^g g(u)\mathrm{d}u \tag{1.24}$$

With $a = 0$, there is no transform at all. With $a = 1$, one finds back the complete equalization (1.21) that yields a flat histogram.

### 1.6.4 Combination and implementation

Histogram equalization has a definite effect on the median gray level. For example, (1.21) will systematically move the initial value $g_m$ to 0.5. However, it is not interesting to tie this correction with a dramatic change of the histogram pattern. The decoupling can be simply achieved if one merges (1.20) and (1.24) into :

$$g'(g) = (1-a)\,q(g) + a\int_0^g g(u)\mathrm{d}u\,, \tag{1.25}$$

that expands as follow :

- $g_a \le g \le g_b$

$$\boxed{\begin{aligned} g'_A(g) &= (1-a)\frac{g-g_a}{g_b-g_m}\left(\frac{g-g_m}{g_b-g_a} + q_m\frac{g_b-g}{g_m-g_a}\right) \\ &+ a\int_0^g\left((1-b)\,h(u) + b\,\frac{\sum w_i^{(A)}H_i(u)}{\sum w_i^{(A)}N_i}\right)\mathrm{d}u \end{aligned}} \tag{1.26}$$

- $\boxed{g'(g < g_a) = 0}$ and $\boxed{g'(g > g_b) = 1}$

where $g_a$, $g_b$ are computed with (1.19).

The parameters of this filter are summarized below :

- $e_a, e_b << 1$ Proportion of pixels to merge at the lower and upper limits of the gray level histogram (e.g. < $10^{-4}$) ;
- $0 < q_m < 1$ Targeted median gray level (e.g. 0.5) ;
- $0 \le a \le 1$ Amount of histogram equalization (e.g. 0.2) ;
- $0 \le b \le 1$ Influence of the local histograms versus global histogram.

In the implementation used for COSMOS, elementary histograms $H$ are computed over contiguous square domains whose side is 64 pixels. Each local histogram $h_A$ is evaluated over a set $A$ made of $(2m+1)^2$ such elementary squares ($9 \times 9$ because $m = 4$). Therefore, a local histogram is used to filter the pixels that belong to the central elementary square of the set $A$. Using a double indexes notation for identifying the elementary domains, (1.23) reads :

$$h_{k,l} = \frac{\sum_{i=-m}^{m}\sum_{j=-m}^{m} w_{ij}H_{k+i,l+j}}{\sum_{i=-m}^{m}\sum_{j=-m}^{m} w_{ij}N_{k+i,l+j}} \quad \text{with} \quad w_{ij} = \max\left(0,\ (m+0.5)^2 - \left(i^2+j^2\right)\right) \tag{1.27}$$

The proposed process is very efficient to spread properly the information to be displayed over the whole gray. Compared to other adaptive filters – such as the Wallis filter – its main drawback is the large amount of memory that may be required to store the many elementary histograms.

### 1.7 A FEW MOSAIC IMAGES

Mosaic images of backscattered echoes have been geo-referenced, commented and interpreted by ICM + IFREMER in the final report on Task 6.1. The mosaic images presented here have been built with a pixel size of 50 cm (the resolution of the printed material in this report is indeed much lower). The selected range of incidence angle is 18° to 78°. The maximal angle is occasionally reduced because of the noise level (see Section 1.2.3 – Figure 1.3). Three areas are displayed in the following :

- Blanes Figure 1.6 (bathymetry Figure 2.11 – Chap.2).
- Vilanova Figures 1.7-8 and 2.12 (bathymetry Figure 2.12)
- Besos Figures 1.9-14 (bathymetry Figures 2.13-14)

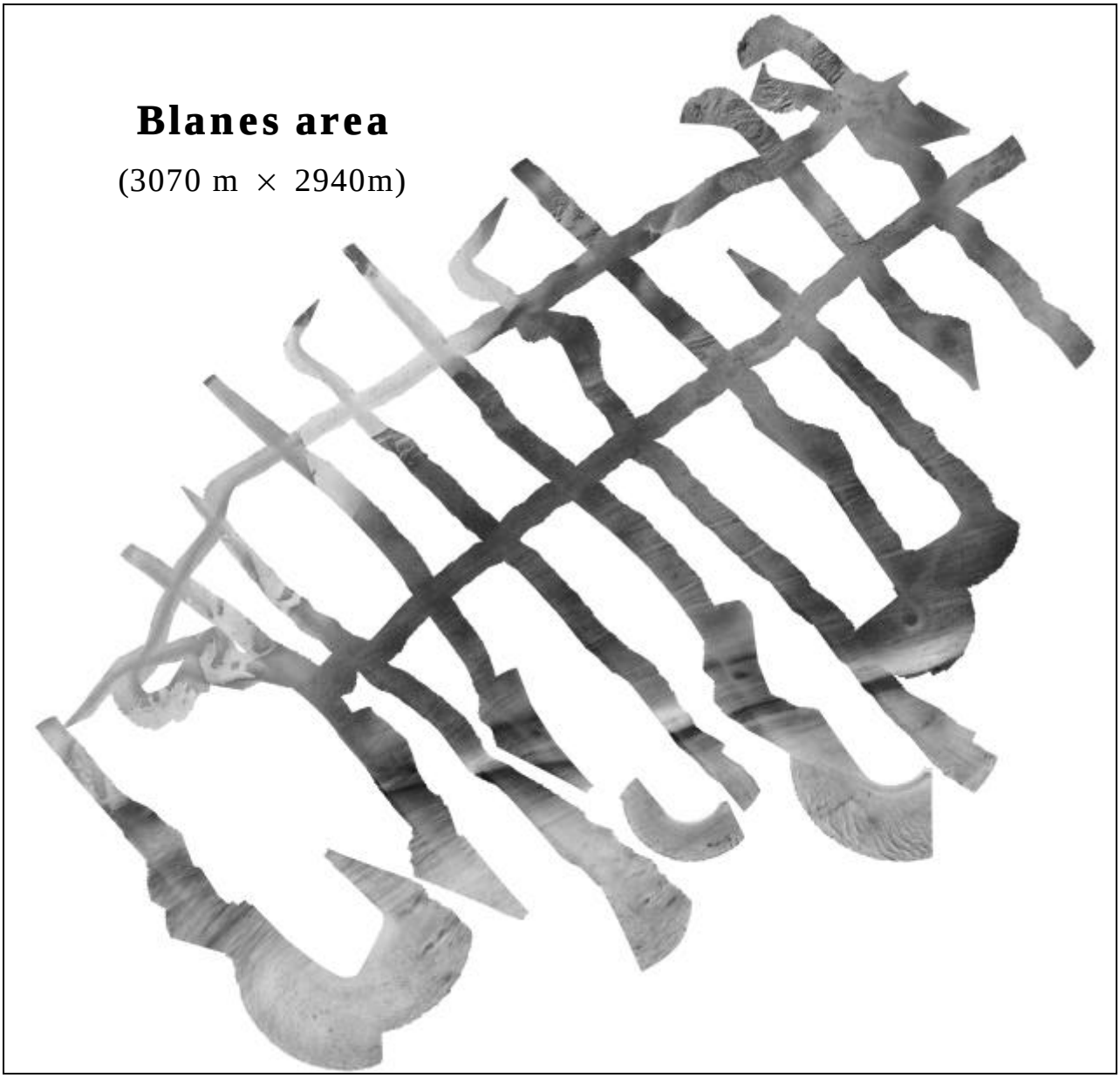


Figure 1.6

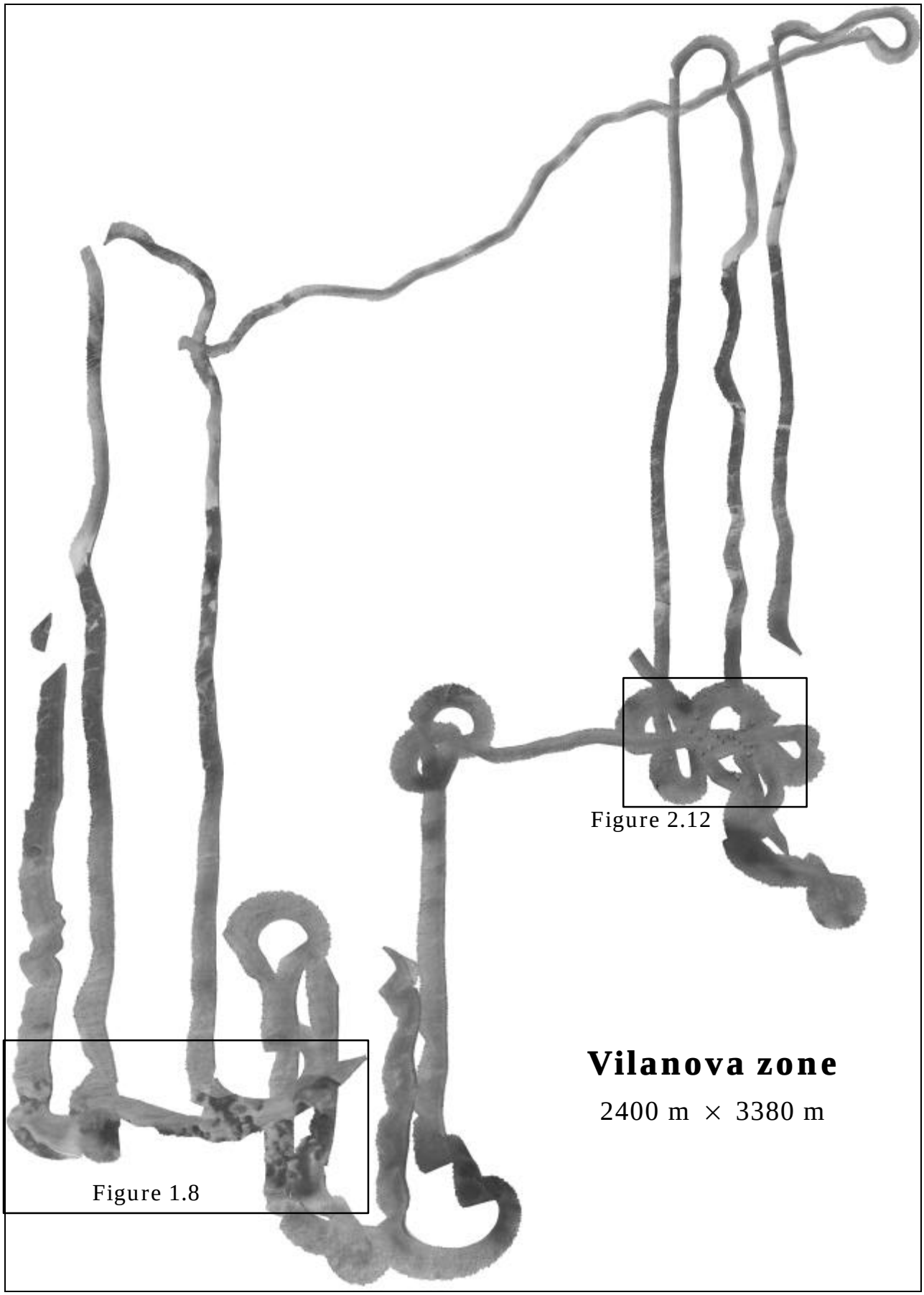


Figure 1.7

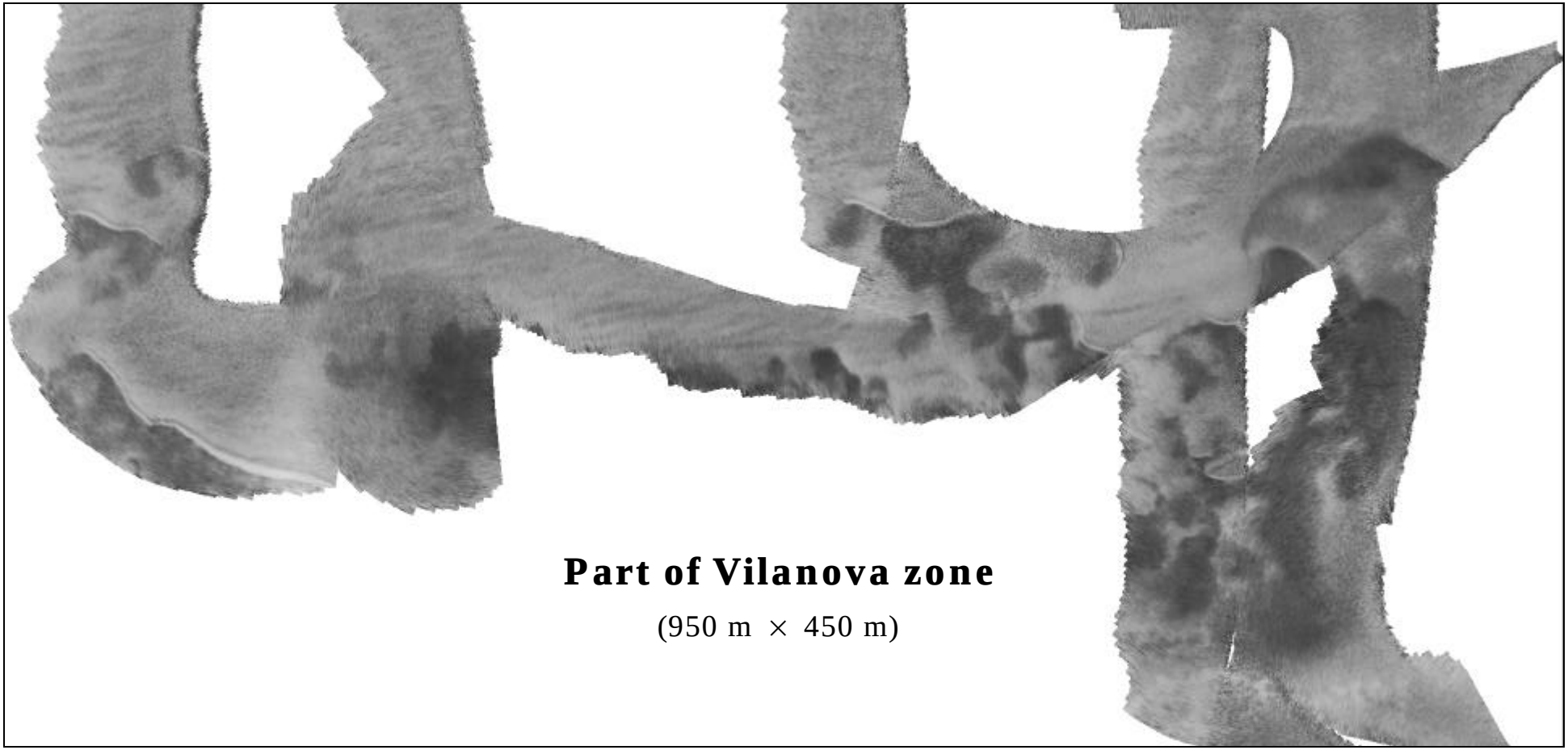


Figure 1.8 : Colonies of posidonia

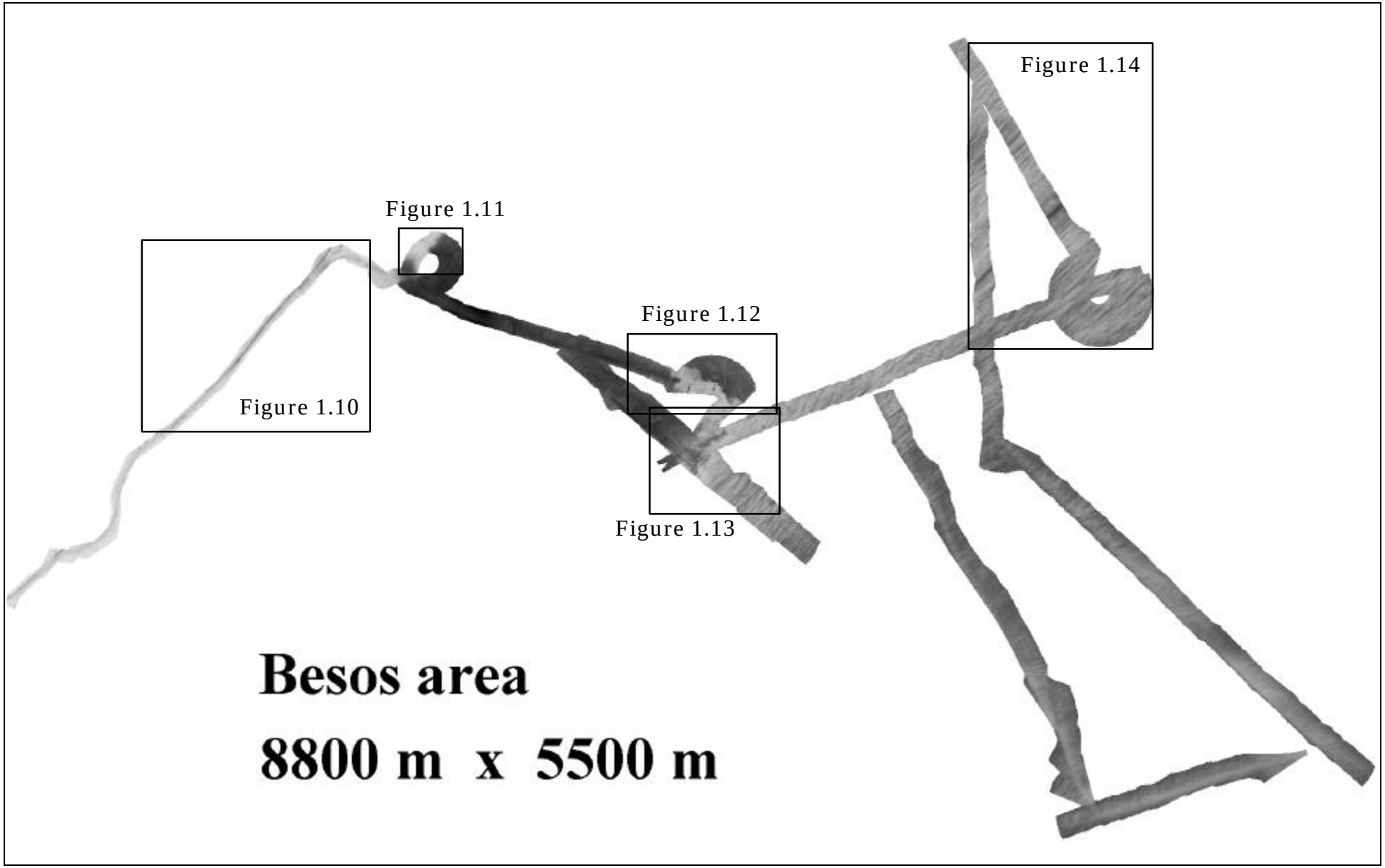
Figure 1.14
Figure 1.11
Figure 1.12
Figure 1.10
Figure 1.13
Besos area
8800 m x 5500 m

Figure 1.9

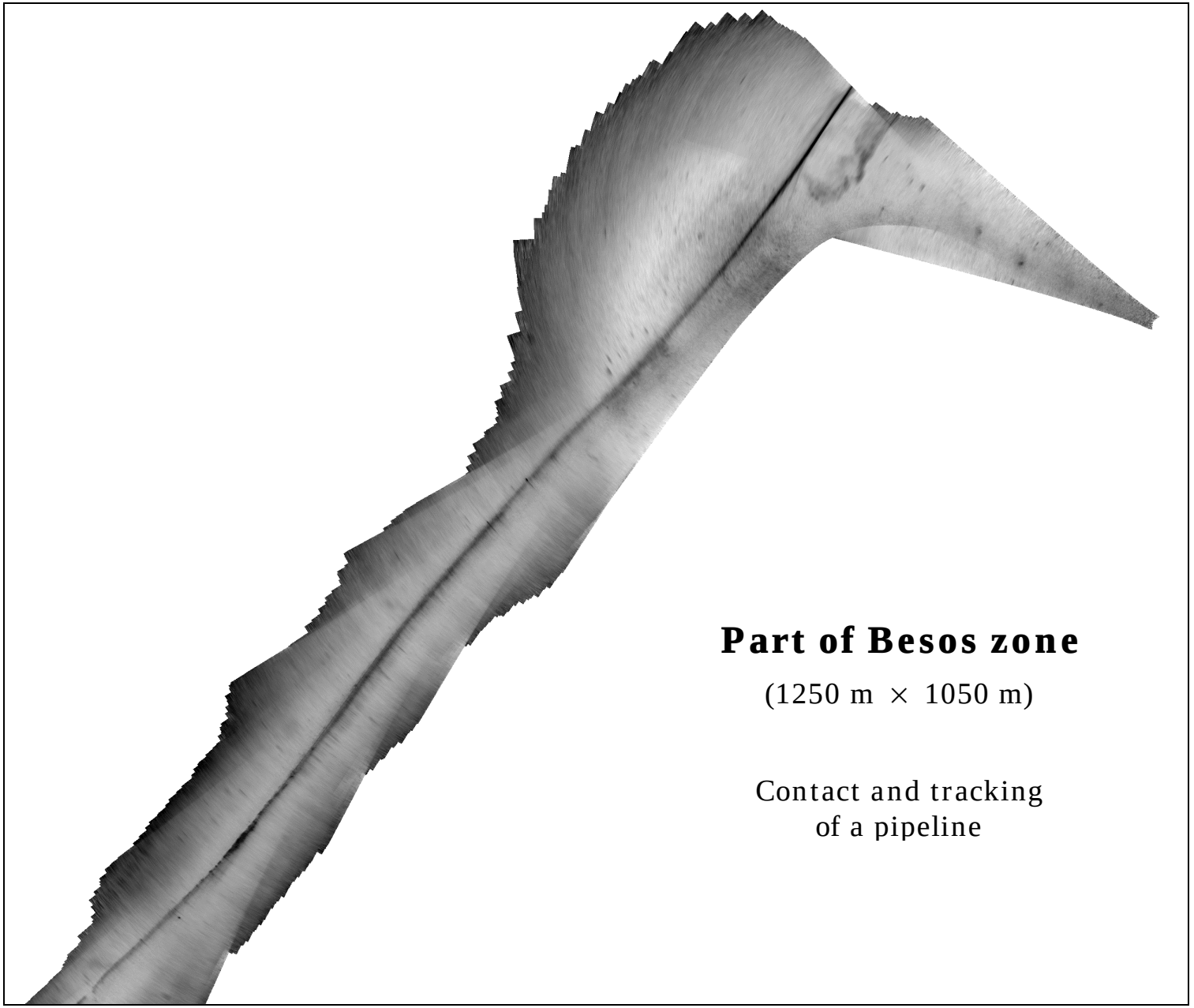
**Part of Besos zone**
(1250 m × 1050 m)
Contact and tracking
of a pipeline

Figure 1.10

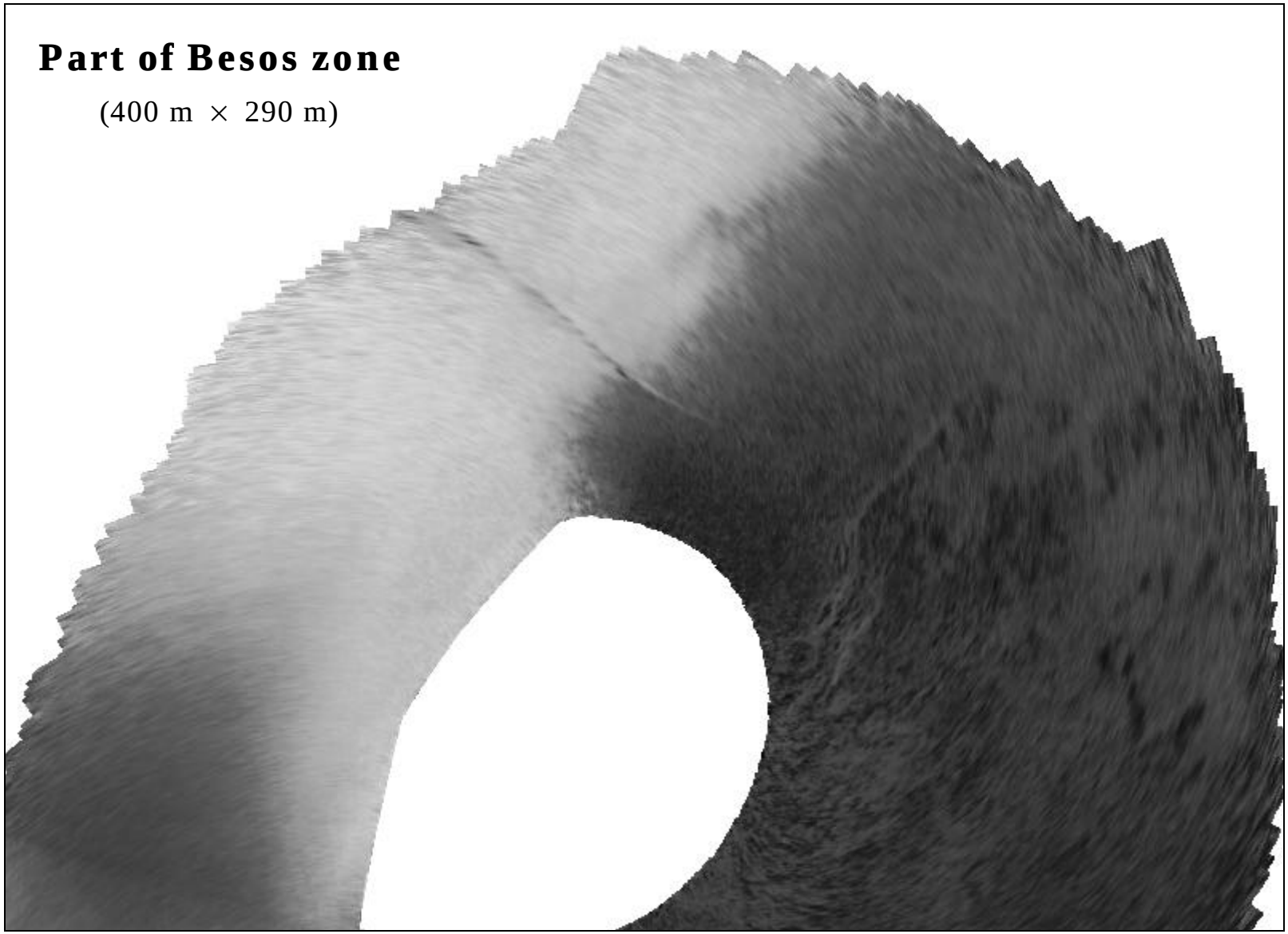


Figure 1.11 : Partially buried pipe

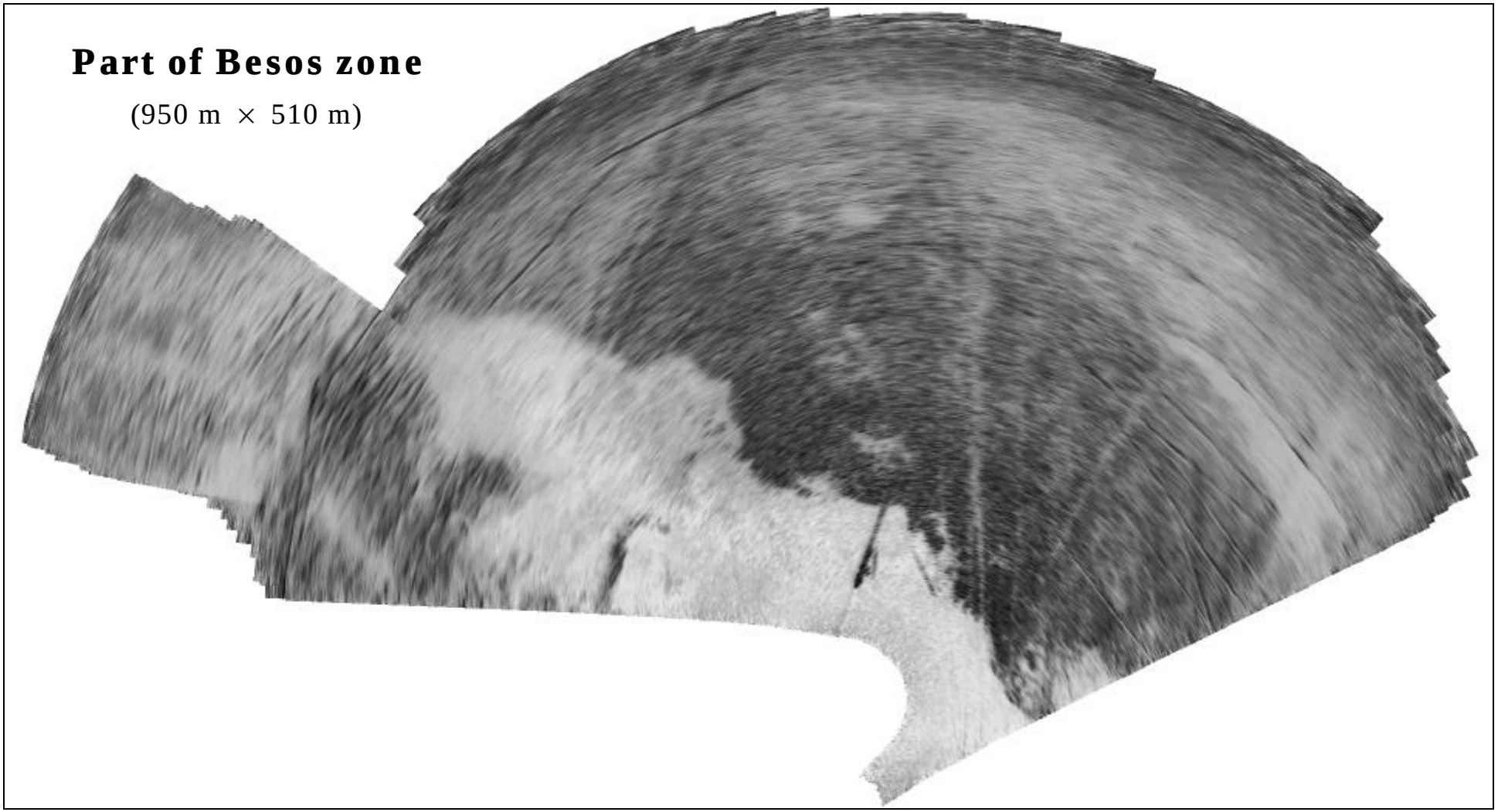


Figure 1.12 : Left turn over an anthropogenic sediment area. Sewer pipe from Barcelona + Trawling marks


Figure 1.13

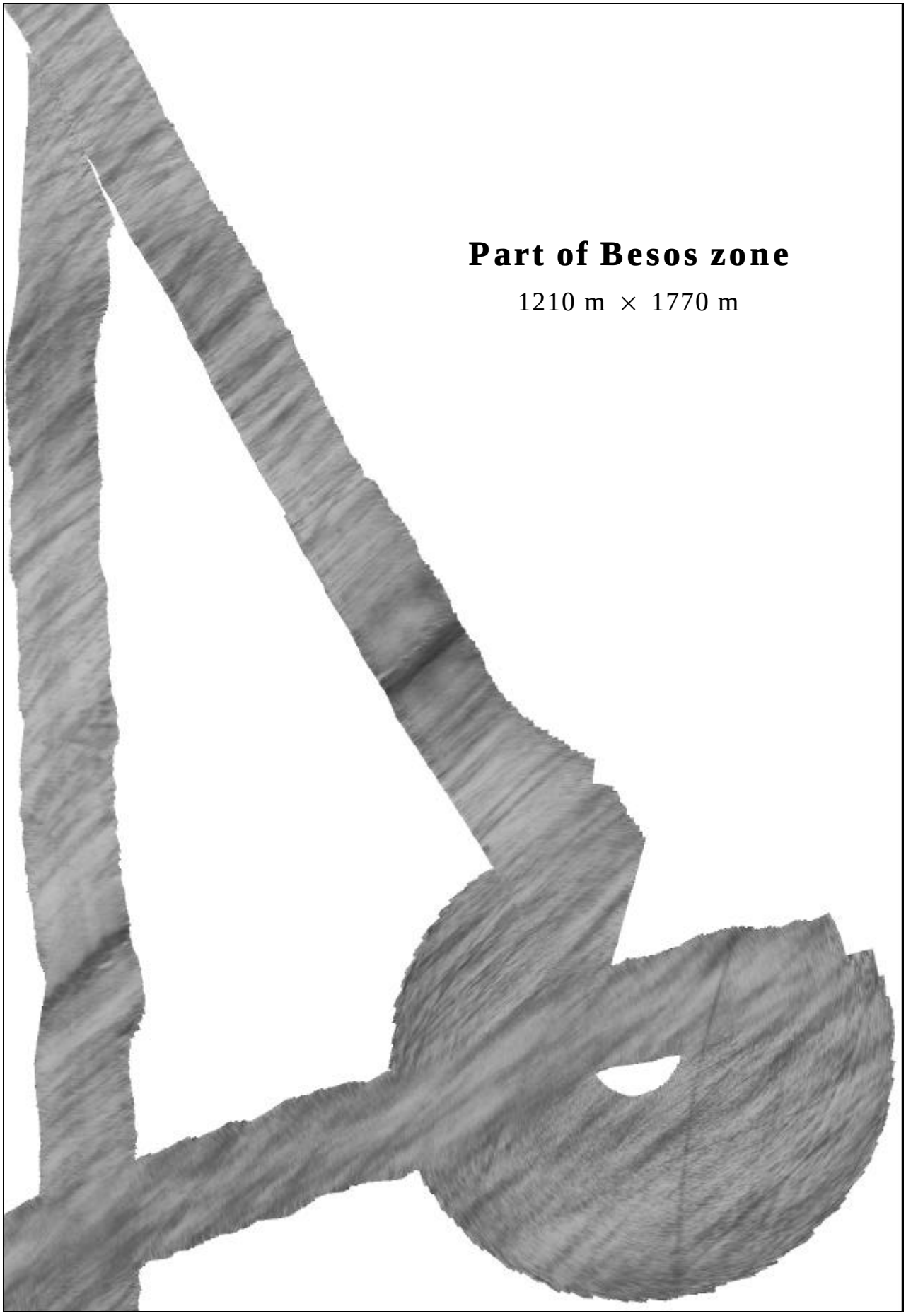


Figure 1.14

# 2. INTERFEROMETRY - BATHYMETRY

The COSMOS system features at receive two linear arrays in order to provide the interferometric capability. The total width in azimuth of the insonified sector is 25°, where $2 \times 31$ beams are formed. Hence, the system can deliver bathymetric data of the scene viewed ahead of the platform.

An interferometer records delayed signals : the relation between differential phases and delays is addressed in Annex 4. To derive soundings, a lookup table is used to convert differential phase angles into geometric angles. The initial calibration of the interferometer is described in Section 1.3.3 of the final report on Task 2 (Figure 1.15). The measurements fit with the theoretical model based on point-like receivers with a baseline equal to 2.13 $\lambda$ (wavelengths @ $c$ = 1500 m/s).

## 2.1 DESCRIPTION OF THE TASK

### 2.1.1 Objectives

The goal of Task 4.2 is to demonstrate that the interferometric process can be combined with a self-calibration technique to derive high quality bathymetry. This technique should refine the lookup table by taking into account the actual conditions of the data collection.

The feasibility to perform in-line the bathymetric function should be assessed.

### 2.1.2 Achievements

- Measurements by interferometry is achieved by estimating the phase difference between received signals, next translated into geometric angles. The validity of the estimate is closely linked to the degree of correlation between these signals. Any interferometric system, characterized by its geometry and the signal used, carries intrinsic causes of decorrelation that are addressed in Section 2.2 through a new, synthetic approach.
- The baseline is larger than $\lambda/2$. Consequently, a phase ambiguity must be removed before conversion into geometric angles. A robust processing technique have been developed to achieve this goal ;
- Another method have been developed to take advantage of the multiple points of view that this system offers. It includes the detection of the biases, and the compensation.
- The compound imaging technique used to build a digital terrain model is also presented.

It has not been possible to make a thorough evaluation of the feasibility to implement the in-line bathymetric function. However, the durations of the post-processing computations that have been observed guaranty that such an implementation depends only on a sufficient effort of development. The computing power of actual PCs seems a priori quite sufficient.

## 2.2 INTERFEROMETRY AND BASELINE DECORRELATION

### 2.2.1 Geometry and Notations

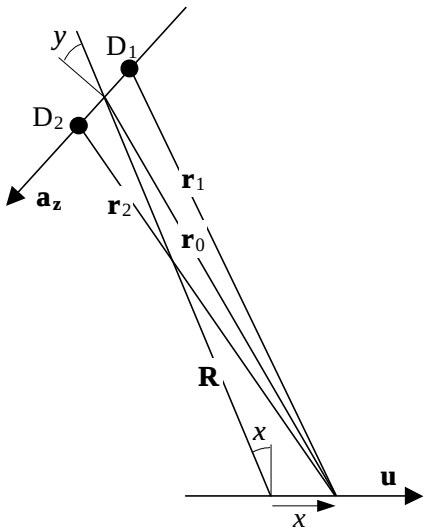


Figure 2.1 : Geometry of the problem (2-D interferometer)

- $D_i$ are the point-like receivers (transmitter located in between)
- $d = |D_1 D_2|$ Baseline
- **u** is the local orientation on the bottom ($x$ : current abscissa)
- **R**, links the interferometer to the origin on the bottom, i.e.
  $\mathbf{R} = R\dfrac{\mathbf{u}\cos y + \mathbf{a_z}\cos x}{\sin(x-y)}$ with $R = ct/2$ ($t$ = 0 : center of signal transmit)
- $\mathbf{r_0}$, $\mathbf{r_1}$ and $\mathbf{r_2}$ link the interferometer to the current point on the bottom, i.e.
  $\mathbf{r}_0 = \mathbf{R} + x\mathbf{u}$, $\mathbf{r}_1 = \mathbf{R_1} + x\mathbf{u} = \mathbf{r}_0 + \frac{1}{2}d\mathbf{a_z}$, $\mathbf{r}_2 = \mathbf{R_2} + x\mathbf{u} = \mathbf{r}_0 - \frac{1}{2}d\mathbf{a_z}$
- $y$ is the incidence angle on the baseline (< 0 in Figure 2.1)
- $x$ is the incidence angle on the bottom ($|x|$ not too small compared to unit)

Note that $\mathbf{a_z}.\mathbf{u} = -\cos(x-y)$.

*In this section, equations numbered (IV.xx) refer to Annex 4.*

### 2.2.2 Signal

The transmitted signal is designed : 1) either to be processed without adapted filter so that it can read as (IV.4) after base-band demodulation ; 2) or to be filtered (e.g. pulse compression) so that it can read as (IV.14). In both cases, let us denote $A(t)$ the resulting processed signal at transmit. According to (IV.5) or (IV.11), the processed signal reads after the delay $r/c$ that corresponds to the time of flight over the distance $r$ : (Attenuation and spreading not taken into account)

$$s(t,r) = A(t - r/c)\exp(-jw_0\, r/c) \tag{2.1}$$

The order of magnitude of the duration of signal $A$ is denoted $T << R/c$

### 2.2.3 Correlation

Let us consider the schematic 2-D configuration pictured in Figure 2.1. The transmitter is located between the point-like receiver $D_1$ and $D_2$. The part of the bottom that is seen at time $t = 2R/c$ is the segment whose direction is given by the axis $\mathbf{u}$, centered around $x\mathbf{u} = 0$. One assumes that the distribution of targets is continuous, with a backscattering strength $w(x)$. The contribution of target $x\mathbf{u}$ to the processed echo received in $D_i$ at time $t_e + 2R/c$, with $|t_e| << 2R/c$, is given by :

$$s_i(x,t_e) = w(x)\, s(t_e + 2R/c,\, r_0 + r_i) \quad (i = 1,2), \tag{2.2}$$

where $w$ is the complex backscattered strength of the elementary targets.

The complete response from the segment reads :

$$S_i(t_e) = \int_{-\infty}^{+\infty} s_i(x,t_e)\, dx\,. \tag{2.3}$$

Denoting $\langle\bullet\rangle$ a statistics performed over many footprints, it is possible to evaluate the mean value :

$$\left\langle S_1(0)\, S_2^*(t_e)\right\rangle = \left\langle \iint w(x)\, w^*(y) \begin{Bmatrix} A\left(\dfrac{2R - r_0(x) - r_1(x)}{c}\right)\exp\left(-jk_0\left(r_0(x) + r_1(x)\right)\right) \\ A^*\left(\dfrac{2R - r_0(y) - r_2(y)}{c} + t_e\right)\exp\left(jk_0\left(r_0(y) + r_2(y)\right)\right) \end{Bmatrix} dxdy \right\rangle \tag{2.4}$$

Let us assume that $w$ is not spatially correlated, and that its phase is random and uniformly distributed :

$$\left\langle w(x) w^*(y)\right\rangle = \left\langle w(x) w^*(x)\right\rangle \delta(y - x) = W^2 \delta(y - x). \tag{2.5}$$

Thus, (2.4) becomes :

$$\left\langle S_1(0)\, S_2^*(t_e)\right\rangle = W^2 \int \begin{Bmatrix} A\left(\dfrac{2R - r_0(x) - r_1(x)}{c}\right) A^*\left(\dfrac{2R - r_0(x) - r_2(x)}{c} + t_e\right) \\ \exp\left(jk_0\left(r_2(x) - r_1(x)\right)\right) \end{Bmatrix} dx\,, \tag{2.6}$$

which reads :

$$\left\langle S_1(0)\, S_2^*(t_e)\right\rangle = W^2 \int A(t_e)\, A^*(t_e + t_e - f) \exp(jw_0 f) \left|\frac{\mathrm{d}x}{\mathrm{d}t_e}\right| \mathrm{d}t_e\,, \tag{2.7}$$

after introducing the new variables :

$$t_e(x) = \frac{2R - r_0(x) - r_1(x)}{c} \quad \text{and} \quad f(t_e) = \frac{r_2(x) - r_1(x)}{c}\,. \tag{2.8}$$

The first order expansion of $t(x)$ reads :

$$ct_e = (R - R_1) - 2x\sin x - x\frac{(R - R_1)\sin x - \frac{1}{2} d\cos(x - y)}{R_1} + O\left(x^2/R\right), \tag{2.9}$$

in which the following order of magnitude applies :

$$R - R_1 = \tfrac{1}{2} d \sin y + O\left(d^2/R\right) \quad << R \tag{2.10}$$

Hence, the order of magnitude of the coefficient for $x$ in the third term of (2.9) is $d/R << 1$. Since $|\sin\xi|$ is not too small compared to unit, this term can be neglected in evaluating $|\mathrm{d}x/\mathrm{d}t|$ :

$$\left|\frac{dx}{dt}\right| \approx \frac{c}{2\sin|x|}. \tag{2.11}$$

Given the fact that $t$ is scaled by $T$, the size of the signal footprint is scaled by $L/\sin x$, with $L = cT$, which remains indeed much smaller than the range $R$. It justifies a posteriori that the incidence angle $x$ is taken as a constant in all these developments.

The first order expansion of $f(x)$ reads :

$$r_2 - r_1 \approx \left(\sin y + \frac{x}{R}\cos x \cos y\right) d \tag{2.12}$$

which translates, by keeping the only terms in (2.9) that bring a significant contribution, into :

$$f\left(t_e\right) = \frac{d \sin y}{c} - \frac{d \cos y}{2R \tan x} t_e \tag{2.13}$$

Within the useful domain of integration (that is sized by the duration of $A(t)$), the variations of $f(t)$ are an order of magnitude smaller than would be required to induce significant variations of $A$. Hence, $f$ can be replaced by the constant f($x$=0) in the argument of $A$ to compute the integrand in (2.7) :

$$A^*\left(t + t_e - f\right) \approx A^*\left(t + t_e - d \sin y / c\right) \tag{2.14}$$

Finally, the integral (2.7) is approximated with :

$$\left\langle S_1(0) S_2^*(t_e)\right\rangle = W^2 \frac{c}{2\sin x} \exp\left(jk_0 d \sin y\right) c_A\left(\Delta t, \Delta n\right) \tag{2.15}$$

using the signal response defined by :

$$\boxed{c_A\left(\Delta t, \Delta n\right) = \int A(t) A^*\left(t + \Delta t\right) \exp\left(-2p\, jt\Delta n\right) \mathrm{d}t} \tag{2.16}$$

with $\boxed{\Delta t\left(t_e\right) = t_e - \frac{d}{c}\sin y}$ and $\boxed{\Delta n = \frac{n_0 d \cos y}{2R \tan x}}$ (2.17)

Let's define the complex correlation factor :

$$g_0 = \frac{\left\langle S_1(0) S_2^*(t_e)\right\rangle}{\sqrt{\left\langle S_1 S_1^*\right\rangle \left\langle S_2 S_2^*\right\rangle}} = \frac{\left\langle S_1(0) S_2^*(t_e)\right\rangle}{S^2} \tag{2.18}$$

where

$$S^2 = \left\langle S_i S_i^*\right\rangle \approx W^2 \frac{c}{2\sin x} c_A(0,0) \tag{2.19}$$

Hence :
$$\boxed{g_0 = \frac{c_A(\Delta t, \Delta n)}{c_A(0,0)} \exp\left( jk_0 d \sin y \right)} \tag{2.20}$$

Note that $\chi_A \chi_A^*$ is the ambiguity function of signal $A$.

$\chi$ can be written in the symmetric form :

$$c_A(\Delta t, \Delta n) \approx \int A(t - \Delta t/2)\, A^*(t + \Delta t/2) \exp(-2p\, jt\Delta n)\, \mathrm{d}t\,, \tag{2.21}$$

as far as it discards a phase term, $\pi \Delta t \Delta n \equiv k_0 d^2/R << k_0 d$, whose order of magnitude is small enough to be neglected in building (2.15).

Whenever $A$ is a real, symmetric signal such as (IV.17), $\chi$ given by (2.21) appears to be also a real function, because being the Fourier transform of a real, symmetric function $F$ :

$$A(t) = A(-t) \in \mathbb{R} \;\Rightarrow\; F(t) = F(-t) = A(t - \Delta t/2)\, A^*(t + \Delta t/2) \in \mathbb{R} \;\Rightarrow\; c \in \mathbb{R} \tag{2.22}$$

Hence, (2.22) implies that (2.20) reads :

$$\boxed{g_0 = |g_0| \exp\left( jk_0 d \sin y \right)} \text{ with } \boxed{|g_0| = \frac{c_A(\Delta t, \Delta n)}{c_A(0,0)}} \tag{2.23}$$

Eq. (2.23) exhibits the important result that the interferometric phase resulting from a base-banded, compressed signal that obeys to (IV.16) is not biased, i.e. one finds back (IV.18) with (IV.3), even when taking into account the multiple interference caused by the finite size of the signal footprint on the bottom.

Let's have a look on the magnitude $|\gamma_0|$ corresponding to two typical signals (rectangular and Gaussian), first exactly, and next with a first order expansion based on the assumption that $|\Delta t| << T$ and $p\Delta n << B = 1/T$ :

- Rectangular signal $A(t) = \mathrm{rect}\left(\frac{t}{T}\right)$ :

$$|g_0| = \mathrm{rect}\left(\frac{\Delta t}{T}\right)\left(1 - \frac{|\Delta t|}{T}\right)\mathrm{sinc}\left(p\Delta n T\left(1 - \frac{|\Delta t|}{T}\right)\right) \approx 1 - \frac{|\Delta t|}{T} - \frac{1}{6}\left(\frac{p\Delta n}{B}\right)^2 \tag{2.24}$$

- Gaussian signal $A(t) = \exp\left(-\left(\frac{2t}{T}\right)^2\right)$ :

$$|g_0| = \exp\left(-\frac{1}{2}\left(\frac{2\Delta t}{T}\right)^2 - \frac{1}{2}\left(\frac{p\Delta n T}{2}\right)^2\right) \approx 1 - 2\left(\frac{\Delta t}{T}\right)^2 - \frac{1}{8}\left(\frac{p\Delta n}{B}\right)^2 \tag{2.25}$$

The developments given in the second parts of (2.24) and (2.25) show that the rectangular signal is more sensitive to time shift (dependency in $\Delta t/T$ ) than the Gaussian signal (dependency in $(\Delta t/T)^2$). This result could be indeed expected because of the "smoother" edges of the Gaussian pattern.

### 2.2.4 Interpretation of result (Eq.(2.20))

- Letting $\Delta t = 0$, the remaining loss of correlation is classically named baseline decorrelation. Scaling to the bandwidth $B$ of the signal, one recognizes that the relative frequency shift is homogeneous to the deviation of the phase differences induced by multiple interferences :

$$\frac{\Delta n}{B} = \frac{Ld\cos y}{2\,l_0 R\tan x} \quad \text{with} \quad B = 1/T\,. \tag{2.26}$$

The ambiguity function that is used in the formulation (2.15) suggests another original interpretation of the phenomenon. Referencing the frequency shift $\Delta n$ to the central frequency $n_0$, one recognizes the equivalent of a Doppler shift caused by the difference in the radial speed of the wave-fronts on the bottom seen from each receiver :

$$\frac{\Delta n}{n_0} = \frac{V_{12}}{c} \quad \text{with} \quad V_{12} = \frac{\mathrm{d}\left(r_1 - r_2\right)}{\mathrm{d}t} = \frac{\mathrm{d}\left(r_1 - r_2\right)}{\mathrm{d}x}\frac{\mathrm{d}x}{\mathrm{d}t} = \frac{d\cos x\cos y}{R}\frac{c}{2\sin x}\,. \tag{2.27}$$

- The time shift $\Delta t(t_e{=}0)$ is caused by the delay between the signals received by each base. Scaling to the signal duration $T$ and equivalent length $L = cT$, the relative time shift is equal to the relative spatial shift of the footprints seen by each receiver, scaled by the size of the footprint :

$$\frac{\Delta t\left(t_e = 0\right)}{T} = \frac{\Delta x = d\sin y\,/\sin x}{\left(L/\sin x\right)} = \frac{d\sin q}{L} \tag{2.28}$$

In other words, the footprints that are simultaneously seen by the receivers do not overlap perfectly : it induces the loss of correlation related to $\Delta t$. This problem can be reduced if the signal processing includes a search for the peak of correlation between the base-banded (filtered, if it applies) signals. This search delivers an estimate, $t_e$, of the delay $t = d\sin y\,/\,c$. This value can be used to derive directly an estimate of the Direction Of Arrival, $y$. The delay $t_e$ can also be used to adjust the signals which thus correlate at best ($\Delta t$ vanishes) to perform the differential phase measurement. Note that if the estimate of the delay is enough accurate, i.e. $\left|t_e - t\right| < p/w_0$, the problem of removing the $2\pi$ ambiguity in the differential phase (if it occurs) is straightforwardly solved.

Actually, the order of magnitude in the accuracy that can be expected for $t$ is $1\,/\,B$, whereas the equivalent figure is rather $1\,/\,n_0$ with the differential phase measurement. The feasibility to implement either scheme (peak of correlation, phase measurement, or combined method) depends mainly on the ratio $B\,/\,n_0$, the scaled baseline $Bd/c$, and the amount of noise.

### 2.2.5 Equivalent noise

Considering other sources of noise and interferences, the magnitude of the complete correlation factor can be interpreted as if both elements of the interferometer would receive a single common signal $s$ that is corrupted by a noise (uncorrelated between the elements). It is assumed that :

- the magnitude of the possible interferences is weak,
- baseline decorrelation remains moderate, i.e. $|\gamma_0|$ is not small compared to 1.
- signal to noise ratio is large

$$|g| = \frac{\left|\left\langle (s+n_1)\left(s\exp(jj)+n_2\right)^*\right\rangle\right|}{\sqrt{\left\langle (s+n_1)(s+n_1)^*\right\rangle\left\langle \left(s\exp(jj)+n_2\right)\left(s\exp(jj)+n_2\right)^*\right\rangle}} \tag{2.29}$$

i.e.

$$|g| = \left(1+N^2/S^2\right)^{-1} \approx \exp\left(-N^2/S^2\right) \tag{2.30}$$

with

$$\left\langle ss^*\right\rangle \approx S^2 << N^2 = \left\langle n_1 n_1^*\right\rangle = \left\langle n_2 n_2^*\right\rangle \text{ and } \left\langle n_1 n_2^*\right\rangle = 0\,, \tag{2.31}$$

where $S^2$ is defined as in (2.19).

Eqs. (2.18) and (2.30) can be related by introducing an additional term $G^2 / S^2$ :

$$N^2/S^2 = -\ln|g| = -\ln|g_0| + G^2/S^2\,. \tag{2.32}$$

The ratio $G^2 / S^2$ accounts for the equivalent noise that degrades the correlation of the signals received at the interferometer, but for the specific contribution of baseline decorrelation. The global coefficient $|g|$ can be estimated experimentally, whereas $|g_0|$ can be computed. Hence, (2.32) allows to derive the equivalent SNR of all other experimental artefacts, i.e. noise in the medium, reverberation, multiple paths.

From a practical point of view, it is important to notice that the variance in the interferometric phase is closely related to the global correlation factor $|g|$ as expressed with (2.30) through :

$$s_j^2 \equiv -\ln|g| = N^2/S^2 \tag{2.33}$$

Relation (2.33) can be shown in a simple theoretical example. It consists of a set of realizations such that the intensity of the echoes does not vary too much around the mean value $S^2$, i.e. :

$$\left\langle \left(ss^* - S^2\right)^2\right\rangle = \left\langle \left(ss^*\right)^2 - S^4\right\rangle << S^4 \cdot$$

In addition, it is assumed that the individual realization of the phase of the received signal reads, after being compensated for its mean value :

$$j = \arg\left(1+n\exp(jV)\right),$$

where $\zeta$ is uniformly distributed in [0,2π[, i.e. $p(V) = 1/(2p)$, noise $n$ is normalized to the average signal level $|S|$, and the variance in $n$ is denoted $\left\langle n^2\right\rangle = \int_{n=0}^{\infty} n^2\, \mathrm{p}(n)\,\mathrm{d}n = N^2/S^2$ .

There is $\Delta j = j_2 - j_1$ so that $\left\langle \Delta j^2\right\rangle = 2\left\langle j_i^2\right\rangle = 2\int_{n=0}^{\infty}\int_{-p}^{+p} p(n)\,p(V)\,n^2 \sin^2 V dV dn$, which gives finally a particular instance of (2.33), i.e. $\left\langle \Delta\varphi^2\right\rangle = \sigma_\varphi^2 = N^2/S^2$ .

### 2.2.6 Numerical figures with COSMOS

#### 2.2.6.1 Equivalent noise

Statistics have been performed on data recorded with the COSMOS system. The correlation factors are computed on selected windows over an homogeneous area. These factors are sorted by incidence angles ($x$) and intensities of backscattered echoes ($S^2$). Given an incidence angle, it has been observed that the correlation factors fit consistently with the following model (variable is $S$) :

$$|g|_x (S) \equiv \exp\left(-N_x^2 / S^2\right). \tag{2.34}$$

Furthermore, the mean coefficient (2.34), have been computed over the experimental distribution of echoes (corresponding to each incidence). Denoting $S_x^2$ the associated mean intensity, the following property is also observed :

$$\left\langle |g|_x \right\rangle \equiv \exp\left(-N_x^2 / S_x^2\right). \tag{2.35}$$

Figure 2.2 exhibits the results of this process, expressed in terms of the equivalent noise to signal ratio $N_x^2 / S_x^2$ (in dB) as a function of the incidence.

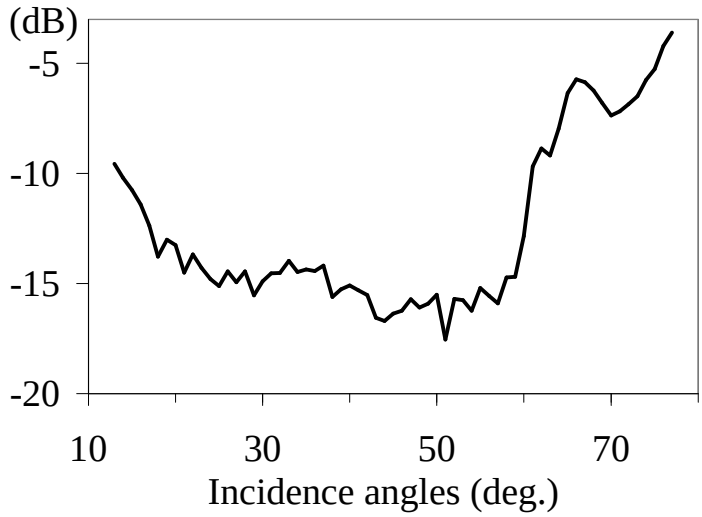


Figure 2.2 : Observed equivalent Noise to Signal ratio

The noise to signal ratio increases sharply beyond 60° incidence : The antennae are close to the surface, so that multiple specular reflections occur between the surface and the bottom. The loss of coherence is likely caused by the induced surge of reverberation.

#### 2.2.6.2 Effect of signal ambiguity

Let us consider the case of a Gaussian signal as given in (2.25), and using (2.17) without any synchronization of the pair of received signals ($t_e = 0$). The variance in phase Eq. (2.33) reads as the following sum of variances :

$$s_j^2 = s_{(j)0}^2 + s_{(j)\text{misc}}^2 \quad \text{with} \quad s_{(j)0}^2 = s_{(j)\text{shift}}^2 + s_{(j)\text{baseline}}^2, \tag{2.36}$$

$$s^2_{(j)\text{shift}} = 2\left(\frac{d\sin y}{L}\right)^2, \quad s^2_{(j)\text{baseline}} = \frac{1}{2}\left(\frac{k_0 L d\cos y}{8R\tan x}\right)^2 \quad \text{and} \quad s^2_{(j)\text{misc}} = G^2/S^2 \qquad (L = cT)$$

Figure 2.3 displays the theoretical contribution of $\gamma_0$, expressed by the equivalent NSR $10\log\left(s^2_{(j)0}\right)$. Compared to the experimental findings shown Figure 2.2, the effect of signal ambiguity seems much weaker. The prevailing causes of the actual loss of correlation are medium reverberation and multiple paths.

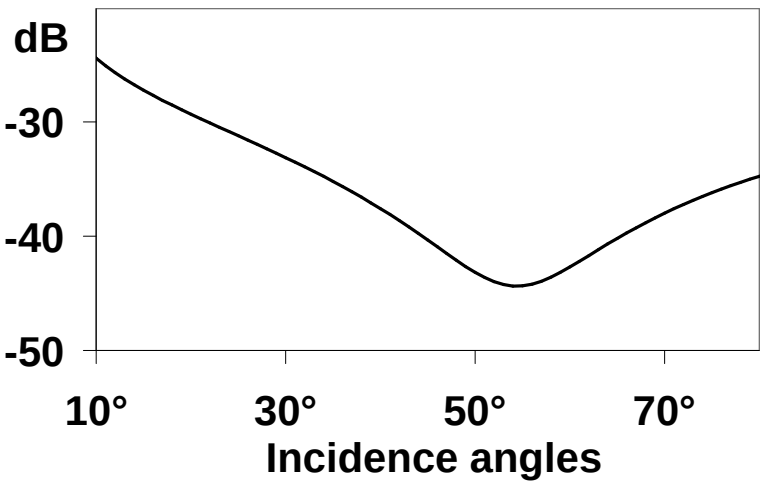


Figure 2.3 : Equivalent Noise to Signal ratio of the correlation factor $\gamma_0$

### 2.2.7 Remark about the effect of signal ambiguity and baseline size

From (2.23) and (IV.3) that link the differential phase and the geometric angle, one derives the corresponding relation with the variances :

$$j = k_0 d\sin y \quad \Rightarrow \quad s^2_y = \frac{s^2_j}{k^2 d^2\cos^2 y}, \tag{2.37}$$

which gives with (2.36) :

$$s^2_y = s^2_{(y)0} + s^2_{(y)\text{misc}} \quad \text{with} \quad s^2_{(y)0} = s^2_{(y)\text{shift}} + s^2_{(y)\text{baseline}} \tag{2.38}$$

$$s^2_{(y)\text{shift}} = 2\left(\frac{\tan y}{kL}\right)^2, \quad s^2_{(y)\text{baseline}} = \frac{1}{2}\left(\frac{L}{8R\tan x}\right)^2 \quad \text{and} \quad s^2_{(y)\text{misc}} = \frac{G^2/S^2}{k^2 d^2\cos^2 y}$$

It can be noticed that the **contribution of the signal ambiguity to the variance in the geometric angle, $s^2_{(y)0}$, does not depend on the baseline size** $d$. On the other hand, $d$ must be set as large as possible as it decreases the influence of other environmental causes such as noise or multiple paths $\left(s^2_{(y)\text{misc}}\right)$. A practical limitation is dictated by the feasibility to solve the $2\pi$ ambiguity : the contribution to the variance in phase, $s^2_{(j)0}$ in (2.36), is proportional to the baseline $d$, and should remain much smaller than $\pi$.

## 2.3 SOUNDINGS

### 2.3.1 Phase processing technique

With COSMOS, the sampling period corresponds to about $\Delta_s \approx 20$ cm in slant range, which is consistent with the radial resolution ($\Delta_r \approx 30$ cm) afforded by the chirp signal. In addition, the baseline ($d \approx 3$ cm) is much smaller than these figures.

Given a ping, let us denote $s_{j(a)}[t_i]$ and $s_{j(b)}[t_i]$ the time sequences corresponding to a single beam (#*j*) formed with each receiving array (*a* and *b*). A systematic search for the peak of inter-correlation between $s_1$ and $s_2$ would be painful (over-sampling needed because $\Delta_s >> d$) and worthless ($\Delta_r >> d$). Hence, the only direct complex conjugate products are considered to derive soundings, i.e. $t_e$ as defined in Section 2.2 is null.

However, a critical issue remains the phase ambiguity removal because $d > l/2$. Differential phase unwrapping algorithms are commonly based on the assumption that the true unwrapped phase field varies slowly enough that in most places, neighboring phase values are within one-half cycle ($\pi$ rad) of one another.

The developed technique takes here advantage of three main factors :

- Usual interferometric side-scan sonar systems are limited to a single dimension (time) in the process. With COSMOS, each ping provides a complete set of adjacent beams, so that data can be processed by following paths in a 2-D space as with synthetic aperture radar interferometry (see for instance Golstein).
- As discussed in Section 2.2, the variance in the differential phases is closely related to the correlation between the signals received by the interferometer. In the devised process, a correlation coefficient is associated to each sample. It allows to sort and to weight reliable data. Considering a single ping, the phase unwrapping is based on a flood-filling technique that avoids areas rejected samples. Properly tuned, most of the processed pings do not exhibit any residue (unwrapped phases gradient greater than $\pi$). Whenever this (rare) situation occurs, the whole ping is withdrawn.
- Successive pings scan sectors than overlap. Consequently, the low-pass filtered unwrapped phase 2-D field does not differ very much from one ping to the next. This property is used to partially compensate for the phase variations before unwrapping.

The main steps of the process applied with the COSMOS system consists of :

- For each beam, the estimated ranges of the first bottom return and of the seafloor at boresight (of the interferometer) are updated. This information allows to double check and to correct the filtered evolution of the unwrapped phases derived from the previous ping. The resulting reference phases are denoted $j_{\text{bias}}[t_i]$.
- The sequences $u_j[t_i] = p_j[t_i]\exp(-jj_{\text{bias}}[t_i])$, with $p_j[t_i] = s_{j(a)}[t_i]s^*_{j(b)}[t_i]$, are built. The phase bias $j_{\text{bias}}$ is introduced to reduce the rate of variation of the phases $\arg(p[t_i])$.
- The sequences $u$ are convolved with a large window $w_L$ whose width increases with range. The resulting complex field is used to derive the unwrapped phases $j_{\text{ref}} = \arg(u * w_L)$. The flood-filling algorithm starts from the ranges corresponding to echoes received at boresight.
- The sequences $u$ are convolved again with another window $w_S$ which is narrower than $w_L$. Within each window, the coefficient of correlation is evaluated and converted into a quality factor $q_j[t_i]$. Phases $j_S = \arg(u * w_S)$ are unwrapped using the field $j_{\text{ref}}$ as a reference, i.e. $|j_S - j_{\text{ref}}| < \pi$.
- Phases $j_S$ are corrected for the bias introduced at the beginning of the process : $j_C = j_S + j_{\text{bias}}$. Figure 2.4 displays an example of sequences $\arg(u)$, $\{j_{\text{ref}}\}$ and $\{q\}$. It can be observed that the quality factor drops severely in the middle of the sequence. It is caused by the arrival of the first specular multiple that occurs when receiving backscattered echoes from an incidence angle of about 60°. In this particular case, a certain amount of information remains usable past this limit.

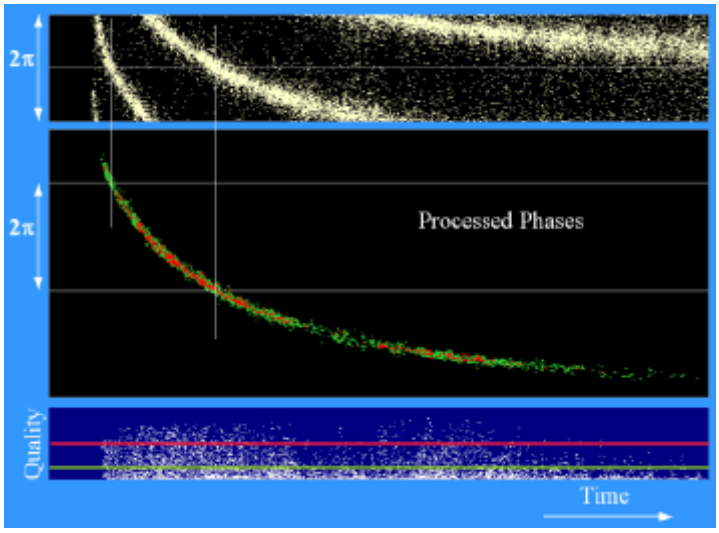


Figure 2.4 : Example of phases before and after processing

- A lookup table is addressed to convert the electric phases into geometric angles. Navigation and attitude data are then merged to derive soundings (see next section) that are recorded together with their quality factors.

### 2.3.2 Positioning

Notations, coordinate systems and rotation matrices are described in Annex 1 ("Data positioning"). In the ACS, the initial direction of a ray, given by the unit vector, **u**, is derived by the intersection of two cones (Figure 2.5). The beam-formed cone is characterized by the angular aperture ($\pi/2 - b$) counted from axis $\mathbf{a_y}$. The beam angle $b$ is null in plane ($\mathbf{a_x}$, $\mathbf{a_z}$) – "flat cone" –, and positive on star-board. The interferometric cone is characterized by the angular aperture ($\pi/2 + y$) counted from axis $\mathbf{a_z}$. The interferometric angle $y$ is negative below plane ($\mathbf{a_x}$, $\mathbf{a_y}$), and positive on the other side.

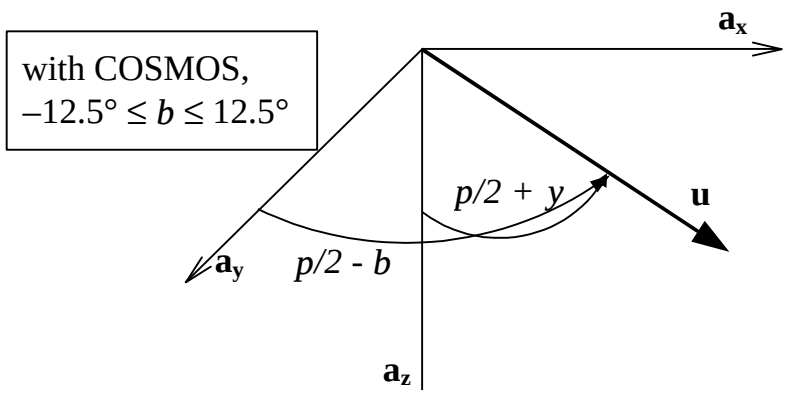


Figure 2.5 : Beamformed and interferometric cones

Whenever the condition $|b| + |y| < \pi/2$ holds, there is :

$$\mathbf{u}_{ACS} = \begin{bmatrix} \sqrt{1-\sin^2 b - \sin^2 y} \\ \sin b \\ -\sin y \end{bmatrix} \tag{3.1}$$

The sequence of operation to derive the FCS coordinates of the direction of an incoming echo is therefore summarized by :

$$\boxed{\mathbf{u}_{FCS} = \mathbf{T}_0\mathbf{T}_1\mathbf{T}_2\mathbf{u}_{ACS}} \tag{3.2}$$

As for imaging, the local origin of coordinates used for each ping is the vertical projection of the GPS antenna onto the sea surface, at ping transmit. Hence, the relative location of the COSMOS module, $O_C$, is approximated with :

$$\mathbf{O}_{\mathbf{C}(FCS)} = \mathbf{T}_0\left[x_0 = -5.3 \quad 0 \quad z_0 = 3.5\right]^t.$$

For each acoustic sample, a ray tracing algorithm, as described in Annex 2, launches a ray from $z_0$ (below the surface), with the cosine of the initial incident angle given by the 3rd component of (3.2). The time of flight is half the round-trip delay. This 2-D process gives the depth and the horizontal distance ($d_h$) of the end of ray, together with the incidence angle at this end. The horizontal location of the sounding is finally obtained by the end of the segment that starts from $O_C$, whose length is $d_h$ and horizontal orientation is the same as vector (3.2). Actually, a complete set of rays are tabulated, so that the additional CPU time needed for taking into account the refraction effect is negligible.

### 2.3.3 Data structure

The program that builds soundings inputs the preprocessed data organized in type ".bms" files. As mentioned in Section 1.3.1, these files are made of "ship_block", "Acou_block" (not used here) and "Phas_block" (Figure 1.4, 1.1, 1.2) blocks. The output consists of type ".xyz" files that collect only "Bath_block" blocks whose structure is shown in Figure 2.6. These blocks consist of a block header, that is followed by two arrays. Each element of the 1st array, **bottom**[], gives the distance, counted in number of time samples, corresponding to the first echo received in the direction of each beam. The 2-D array, **bathymetry**[], contains the soundings, one line per beam ; the first element of a line corresponds to the sample index #hit_index.

```
typedef struct {
  def_packet_id packet_id;  // sizeofpacket = sizeof(def_bath_hd) + bath_hd.nb_beams*sizeof(short)
                            //                + bath_hd.nb_beams*bath_hd.nb_tixels*sizeof(def_bathy)
                            //   typeofpacket = Bath_pk
  long  status;             //
  long  longitude;          // 1.e7 * longitude (in decimal degrees)      (W <0, E >0)
  long  latitude;           // 1.e7 * latitude (in decimal degrees)       (S <0,  N >0)
  short hit_index;          // (in tixels)  equivalent to acou_hd.depth_index, i.e. 1st bottom return index
  short x_unit;             // mm
  short y_unit;             // mm
  short z_unit;             // mm
  short anten_x;            // Position of the antenna at transmit,  in x_, y_ and z_units :
  short anten_y;            //   Origin is the vertical projection of theGPS antenna
  short anten_z;            //       at the sea surface
  short inc_min;            // 10000 * min incidence angle (rad) for interferometry
  short aperture;           // 10000 * aperture (in rad)                  (default :  4363)
  short site_mount;         // 10000 * site_mount_angle (<0, in rad)      (default : -6457)
  short azi_mount;          // 10000 * azi_mount_angle  (in rad)          (default :    305)
  short nb_beams;           // default : 31
  short nb_tixels;          // Starting index for (def_bathy) data is hit_index,
                            //      i.e. tixel range is [hit_index, hit_index + nb_tixels - 1]
} def_bath_hd;

typedef struct {
  short x;                  // in x_unit
  short y;                  // in y_unit
  short z;                  // in z_unit
  short inc_up;             // 10000 * incidence angle (rad) close to antenna
  short inc_ed;             // 10000 * incidence angle (rad) at the end of ray
  short sinitf;             // 10000 * sin(interferometric angle)
  short q;                  // Quality (unit = 1/32765)
} def_bathy;

//  Bath_block {            // For info only. This is NOT a C structure
//    def_bath_hd  bath_hd;
//    short        bottom[bath_hd.nb_beams];
//    def_bathy    bathymetry[bath_hd.nb_beams][bath_hd.nb_tixels];
//  }
```

Figure 2.6 : Structure of blocks concerning bathymetry

## 2.4 INTERPOLATION AND MAPPING

The technique to build mosaic images of soundings is very similar to the one used for imaging the backscattered strength. The map management and interpolation process are identical (Annex 3). Let us consider the record of a ping whose data are organized as several sequences of time samples. Each sequence corresponds to a formed beam (line of **bathymetry[]**). We focus on three pieces of information carried by each individual sample :

- $z$ in fine, the value of interest
- $q$ a quality factor (based on a correlation coefficient)
- $a$ a sorting criterion data, e.g. the interferometric angle (sinitf)

The interpolation scheme maps each ping onto the local grid (P space). It consists of the elements ($q$, $qz$, $a$).

The survey space S consists of 32 mosaic layers. One layer is dedicated to data related with first bottom returns of all beams. The 31 other layers carry data derived by interferometry : each layer corresponds to a small range of the sorting parameter $a$. The ping map P is dispatched into the active window S. Within each layer, data are stacked in a structure made of 3 elements : a weighted sum of soundings $(qz)_{pi}=\Sigma qz$ ; the sum of the corresponding weights $q_{pi}=\Sigma q$ ; and the sum of the following combinations :

$$v_{pi} = \Sigma q^2 \ln q. \tag{4.1}$$

Once all the pings are processed and data stacked in the layers, an additional, final, layer is build by summing the elements of a chosen set of layers :

$$(qz)_p = \sum_i (qz)_{pi}\,, \quad q_p = \sum_i q_{pi}\,, \quad v_p = \sum_i v_{pi} \tag{4.2}$$

where $p$ and $i$ are indexes relative to the pixel and the layer, respectively.

The expected depth is then derived by :

$$\boxed{Z_p = (qz)_p / q_p}. \tag{4.3}$$

A consistent quality factor of the above estimate is obtained with :

$$\boxed{Q_p = \exp\left(v_p / q_p^2\right)}. \tag{4.4}$$

The starting point of formulae (4.1) and (4.4) is the definition of the quality factor. The element "$q$" of the structure "def_bathy" is defined by :

$$q = 32766\, g^{\ln(2)/j_{\text{mean}}^2}\,. \tag{4.5}$$

where $g$ is the measured local intercorrelation coefficient, and $j_{\text{mean}}$ = 0.1 rad.

It has been discussed in Section 2.2.5 than the coefficient of correlation $g$ and the variance in differential phase are closely related through (2.33). Although corrective factors that depend for

instance on the incidence angle should be taken into account, one can reasonably extrapolate the same kind of relation with the variance in depth :

$$g = \exp\left(-a\, s_z^2\right), \tag{4.6}$$

where $a$ is a factor whose order of magnitude is the unit but the exact value is not known. Consequently, (4.5) reads :

$$q \equiv \exp\left(-b\, s_z^2\right) \;\Rightarrow\; s_z^2 \equiv -b^{-1} \ln q\,, \tag{4.7}$$

where $b$ is another unknown, constant value. The variance in the weighted sum of uncorrelated samples (4.3) is therefore the following sum of elementary variances :

$$s_Z^2 = \sum\left(\frac{q}{\sum q}\, s_z\right)^2 \equiv -b^{-1}\frac{\sum\left(q^2 \ln q\right)}{\left(\sum q\right)^2}. \tag{4.8}$$

Applying the same relation as (4.7) for assigning a global quality factor to the mean depth $Z$, one finds back (4.4), i.e. :

$$\ln Q = \frac{\sum\left(q^2 \ln q\right)}{\left(\sum q\right)^2} \;\Rightarrow\; Q = \exp\left(\frac{\sum\left(q^2 \ln q\right)}{\left(\sum q\right)^2}\right) \tag{4.9}$$

This final quality factor can be used to select the gridded soundings that make a digital terrain model of the surveyed area. In addition, the quality factor can be used as a weighting factor if a low pass filtering is needed.

The superimposition of layers depicted here is meant to reduce the variance of the resulting soundings. However, this goal cannot be reached if there are biases in the measurements, i.e. if systematic mismatches between mosaic layers occur. The next section is devoted to this problem.

## 2.5 SELF CALIBRATION

### 2.5.1 Search for bias

Soundings obtained by interferometry can be biased because of various effects. For example, the bias can be caused by errors in the bathycelerimetry profile (including the effect of the temperature close to the antenna), or in the attitude of the platform. With COSMOS, each ping provides a whole set of soundings derived from many different points of view. Hence, the redundancy gives a powerful hint for detecting such biases. After correction, the superimposition of many soundings leads to reduce the influence of the variance in the measurement. A method is devised here to evaluate the bias, assuming that soundings are sorted according to a chosen criterion (e.g. interferometric or grazing angles).

Let us denote **Z** the matrix that is built with measured soundings. Size of **Z** is $m$ rows $\times$ $n$ columns. Each line corresponds to a pixel for which at least 2, and no more than $n$, soundings are available. Each column corresponds to a given range in the selected criterion (e.g. the interferometric angle). Each sounding is also attributed a quality factor ($0 \le w \le 1$) which is collected in matrix **W** (same size as **Z**). Null elements of **W** correspond to unavailable data in **Z**.

The reduced matrix **S** is derived by building the zero-mean relative soundings computed with regard to each pixel :

$$s_{pq} = \frac{z_{pq} - \overline{z}_p}{\overline{z}_p} \quad \text{with} \quad \overline{z}_p = \frac{\sum_i w_{pi} z_{pi}}{\overline{w}_p} \quad \text{and} \quad \overline{w}_p = \sum_i w_{pi} \tag{5.1}$$

Hence, **S** is defined such as :

$$\forall p, \quad \sum_q w_{pq} s_{pq} = 0 \,. \tag{5.2}$$

We are looking for the vector **B** whose $n$ components describe the bias in the soundings as a function of the chosen criterion (e.g. the interferometric angle). Unbiased soundings $z'$ should be recovered by making :

$$z'_{pi} = z_{pi} \big/ \left(1 + b_i\right), \tag{5.3}$$

Hence, the problem consists of fitting the lines of **S** with the transposed of **B**. It is assumed that all components of **B** are very small compared to unit. A least square fitting is built by using the following cost function :

$$K^2 = \sum_p \sum_i w_{pi} \left( s_{pi} - \left( b_i - \overline{b}_p \right) \right)^2 \tag{5.4}$$

Within the contribution of each pixel ($p$) that builds the cost function given in (5.4), all the components of the model are compensated by $\overline{b}_p$ for taking into account the shift in the local mean sounding that the weighting introduces. Hence, these offsets are computed according to :

$$\sum_q w_{pq}\left(b_q - \bar{b}_p\right) = 0\,,\ \text{ i.e. }\ \bar{b}_p = \frac{\sum_q w_{pq} b_q}{\bar{w}_p} \tag{5.5}$$

Least square fitting amount here to solve the following system :

$$\partial K^2 / \partial b_i = 0 \quad (i = 0,\ldots,n\text{-}1) \tag{5.6}$$

Eqs.(5.6) reduce to :

$$\sum_p w_{pn}\left(s_{pn} - b_n + \bar{b}_p\right) = 0 \tag{5.7}$$

which gives finally :

$$\boxed{-\sum_q b_q \sum_p \frac{w_{pn} w_{pq}}{\bar{w}_p} + b_n \sum_p w_{pn} = \sum_p w_{pn} s_{pn}} \tag{5.8}$$

It can be noticed in (5.4) that $K^2(\{b_i\}) = K^2(\{b_i + \alpha\})$, so that **an additional independent condition must be added to solve the system (5.8)**, e.g $b_0 = 0$.

### 2.5.2 Variances

Using (5.7), it can be shown that :

$$K^2 = \sum_p \sum_i w_{pi} s_{pi}\left(s_{pi} - b_i\right) \tag{5.9}$$

so that the global variance can be expressed with :

$$\boxed{s^2 = \frac{K^2}{\sum_p \sum_i w_{pi}} = \frac{\sum_p \sum_i w_{pi} s_{pi}^2 - \sum_i \left( b_i \sum_p w_{pi} s_{pi} \right)}{\sum_p \sum_i w_{pi}}} \tag{5.10}$$

This variance can also be split into a sum of variances. Each contribution quantifies the “noise” of an individual mosaic layer with respect to the global digital terrain model :

$$s^2 \sum_p \sum_i w_{pi} = \sum_i \left( s_i^2 \sum_p w_{pi} \right) \ \text{ with }\ s_i^2 \sum_p w_{pi} = \sum_p w_{pi}\left(s_{pi} - b_i + \bar{b}_p\right)^2 \tag{5.11}$$

These parameters can be expressed as :

$$s_i^2 \sum_p w_{pi} = \sum_p w_{pi}\left(s_{pi} + \bar{b}_p\right)\left(s_{pi} - b_i + \bar{b}_p\right) \tag{5.12}$$

which can reduce to :

$$\boxed{s_i^2 = \frac{\sum_p w_{pi}\left(s_{pi} + \bar{b}_p\right)^2}{\sum_p w_{pi}} - b_i^2} \tag{5.13}$$

### 2.5.3 Compensation for bias

Let us consider the original lookup table (conversion from phase angles $j$ into geometric angles $y$) used for building a set of soundings :

$$y = y_0(j) \tag{5.14}$$

We assume that the set of sounding is sorted by interferometric angle $\{z(y)\}$. Using the statistical analysis described in the previous section 2.5.1, the following bias is estimated :

$$\boxed{b(y) \simeq \frac{\Delta z}{z}(y)}, \tag{5.15}$$

where $\Delta z = z - z'$, $z'$ being the unbiased sounding.

The question that is addressed here is the correction $\Delta y(y)$ that must be applied to the lookup table (5.14) so that new soundings derived by means of the corrected table $y_1(j)$ would exhibit a significantly reduced bias :

$$y_1(j) = y_0(j) + \Delta y\left(y_0(j)\right) \tag{5.16}$$

Let us denote $n_z$ the third component of the unit vector $\mathbf{u}_{\mathrm{FCS}}$ (3.2) that gives the direction of each target (no refraction, no heave). The correction $\Delta y$ that must be applied to the interferometric angles in order to reduce the bias described by (5.15) is :

$$\Delta y = -Cb(y) \tag{5.17}$$

with

$$C = \frac{n_z}{\partial n_z / \partial y} \tag{5.18}$$

With a null heading ($h = 0$), a perfect along-track mounting of the antennae ($l = 0$), and neutral attitude angles ($p = r = 0$), the transform matrices (I.1-3) reduce to :

$$\mathbf{T}_0 = \mathbf{T}_1 = \mathbf{I} \quad \text{and} \quad \mathbf{T}_2 = \begin{bmatrix} \cos m & 0 & \sin m \\ 0 & 1 & 0 \\ -\sin m & 0 & \cos m \end{bmatrix} \tag{5.19}$$

so that $\mathbf{u}_{\mathrm{FCS}}$ (3.2) becomes :

$$\mathbf{u}_{FCS} = \begin{bmatrix} n_x \\ n_y \\ n_z \end{bmatrix} = \begin{bmatrix} \cos m\sqrt{1-\sin^2 b - \sin^2 y} - \sin m \sin y \\ \sin b \\ -\sin m\sqrt{1-\sin^2 b - \sin^2 y} - \cos m \sin y \end{bmatrix} \tag{5.20}$$

The problem in evaluating (5.17) is that $n_z$ depends also on the beam angle, $b$ :

$$C = C(y, b) = -\frac{\left(\cos m \sin y + \sin m\sqrt{1-\sin^2 b - \sin^2 y}\right)\sqrt{1-\sin^2 b - \sin^2 y}}{\left(\sin m \sin y - \cos m\sqrt{1-\sin^2 b - \sin^2 y}\right)\cos y} \tag{5.21}$$

It can be verified that :

$$C(y,0)=\tan(m+y),\quad \left.\frac{\partial C}{\partial b}\right|_{b=0}=0,\quad \text{and}\quad \left.\frac{\partial C}{\partial^2 b}\right|_{b=0}=-\frac{\sin m}{\cos^2 y}\frac{\cos(2y+m)}{\cos^2(y+m)} \tag{5.22}$$

so that the development of (5.21) with respect to $b$ up the second order reads :

$$C(y,b)\approx\tan(y+m)\left(1-\frac{\sin m}{\cos^2 y}\frac{\cos(2y+m)}{\sin(2y+2m)}b^2\right) \tag{5.23}$$

The aperture in azimuth of the COSMOS system is relatively small, i.e. :

$$\left|1-\frac{\sin b_{\max}}{b_{\max}}\right|<10^{-2}\ll 1 \tag{5.24}$$

Hence, the maximal relative difference between the off-axis ($b \neq 0$) and the along-track ($b = 0$) values taken by $C$ is also small. Assuming that the system delivers samples that are uniformly distributed over all the beams, the following average coefficient can be considered to implement the correction :

$$\boxed{C(y)=\frac{1}{b_{\max}}\int_0^{b_{\max}}C(y,b)\,\mathrm{d}b\approx\left(1+E(y)\right)\tan(y+m)} \tag{5.25}$$

with

$$\boxed{E(y)=-\frac{\sin m}{\cos^2 y}\frac{\cos(2y+m)}{\sin(2y+2m)}\frac{b_{\max}^2}{3}} \tag{5.26}$$

Figure 2.7 shows the evolution of $E(y)$, with $\mu = -37.5°$ and $b_{\max} = 12.5°$. The interferometric angle $y$ runs from –42.5° to 27.5°, which corresponds – in the along-track vertical plane – to grazing angles that run from 80° (close to nadir) to 10°.

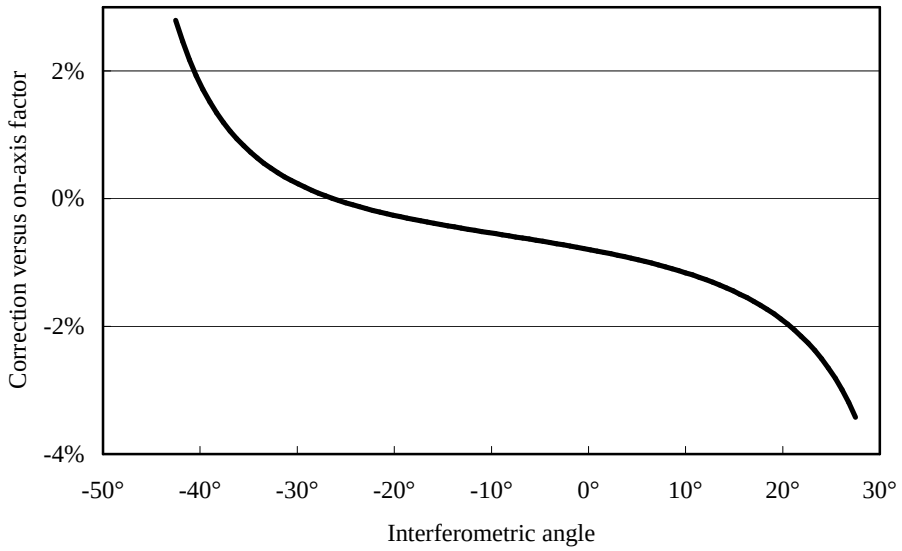


Figure 2.7 : Compensation in the along-track evaluation of the correction

**Summary** : Given a bias $b(y)$ (c.f. (5.15)), the lookup table is corrected according to (5.16). The correction is evaluated with the product given in (5.17), in which the coefficient $C$ is approximated with (5.25) and (5.26).

### 2.5.4 Examples

Several legs have been selected in the "Blanes" area to perform the above described statistics. These legs feature a large variety of depths (15 m to 65 m) and slopes. The initial mosaics are built with the nominal mounting angle ($\mu = -38.5°$) and with the theoretical lookup table. The biases and the deviations, evaluated according to (5.8) and (5.13) respectively, are displayed Figures 2.8a-b. The biases are much larger than the deviations, so that there is indeed a significant interest in the reduction of the former.

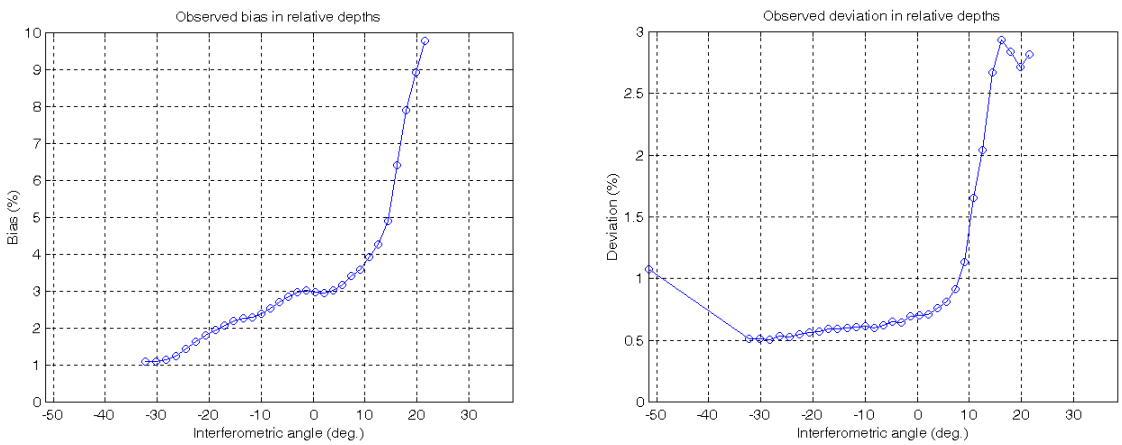


(a) Bias (b) Deviation

Figure 2.8 : First pass

To this purpose, a correction in the lookup table is derived by (5.17)-(5.25) from the biases. It can be noticed in Figure 2.9 that the mean value of the correction ($\approx 1.5°$) is larger than its range of variation (a few tenth of degrees). It suggests that the assumed mounting angle is not correct. Hence, this parameter is changed in the next iteration ($\mu = -37°$). Accordingly, the correction shown Figure 2.9 is shifted down by 1.5° in the actual implementation of the new lookup table.

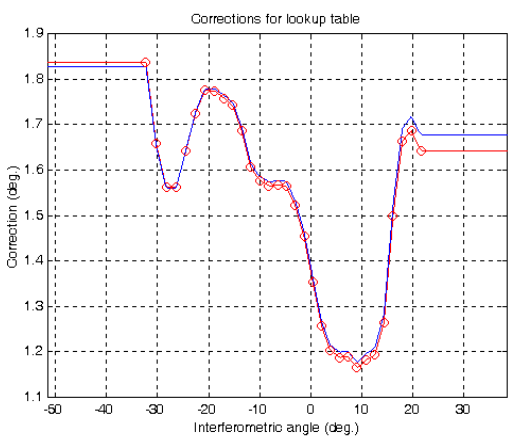


Figure 2.9 : Correction derived from biases at the first pass

Multi-layer mosaic are rebuilt with the new settings, and statistics are again computed. The deviations (Figure 2.10b) remain almost identical to the figures

obtained at the previous step (Figure 2.8b). On the other hand, Figure 2.10a shows that the biases are reduced by more than one order of magnitude (versus Figure 2.8a). Hence, the biases are now negligible compared to the deviations. The goal is reached. Another iteration would be meaningless.

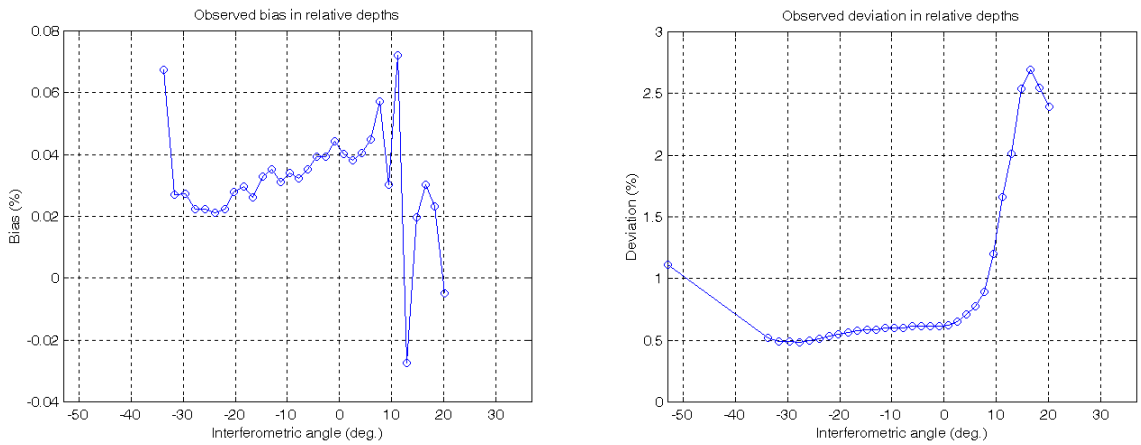


(a) Bias (b) Deviation

Figure 2.10 : Second pass

On the other hand, the estimate of the deviation delivers another interesting information. The COSMOS module was operating close to the surface. This situation is known (with interferometric sidescan sonar systems) to forbid any useful measurement past an incidence angle of 60° : echoes following multiple paths (e.g. antenna / bottom / surface / bottom / antenna) start to interfere with the direct backscattered signals. This phenomenon is clearly visible in Figures 2.8b and 2.10b, where the deviation increases sharply past an interferometric angle in the range 5°– 10°.(equiv. incidence : 90° – 37° + **7°** = 60°)

Consequently, the advantage of the redundancy afforded by the COSMOS system is twofold in the interferometric application : 1) it allows to calibrate the system, i.e. the bias related to the angle of view can be canceled ; 2) the operational range for the interferometric angle can be properly defined because the deviation in the measurements versus the angle of view can be quantified.

## 2.6 A FEW MAPS

The first layer (deviation ≈ 1.1%) in Figures 2.8b and 2.10b corresponds to the soundings obtained by the first bottom returns, i.e. these data are not obtained by interferometry. The deviation in this mosaic layer (#0) is larger than 1%. Consequently, layer #0 is discarded to build final digital terrain models.

Accordingly, digital terrain models presented here are built with the only first 24 layers (#1 – #24) – from 31 available – whose deviation is smaller than 1%. The order of magnitude of the resulting global deviation, as estimated with (5.10) , is a few tenths of percent.

All maps are built with a pixel size of 1 m × 1 m. With such a resolution cell, the residual noise is such that data should be filtered before contouring. The maps presented here are coded with colors, because they do not require such filtering.

One must be also aware that the presented results can be offset compared to other data sets. Possible sources for the bias are listed below :

1) No compensation has been introduced for the actual sea level at the time of the survey (tide, atmospheric pressure, wind). It introduces an additive bias in the COSMOS bathymetry.

2) The order of magnitude of the accuracy in the positioning of the COSMOS wet module under the surface is rather in the decimeter than in the centimeter.

3) There is a (small) multiplicative bias in the COSMOS bathymetry. As explained at the end of Section 2.5.1, the self-calibration procedure is efficient but for an additive constant factor – counted in relative depth – that remains unknown. The order of magnitude of this error is limited to a few parts per thousand, i.e. definitively less than the percent.

Figure 2.11 is the Blanes zone. The self calibration technique has been studied with data from this zone.

Figure 2.12 is part of the Vilanova zone. Several artificial reefs are laid on the bottom. They are 3 m × 3 m × 3 m cubes. The data processing introduces a smoothing effect, so that the terrain model does not exhibits 3m high bumps. However, the artificial reefs are definitively detected. The order of magnitude of the apparent height is the meter.

Figures 2.13-14 displays part of the Besos zone. Two cones are visible. They are mud “volcanos”. The smaller one (NW of the picture) is probably caused by a leak in the sewer pipe that crosses the area. The main cone corresponds to the output of the sewer. It is more than 8 m height from its base. There is a depression at the center, about 2 m deep (from the upper rim).

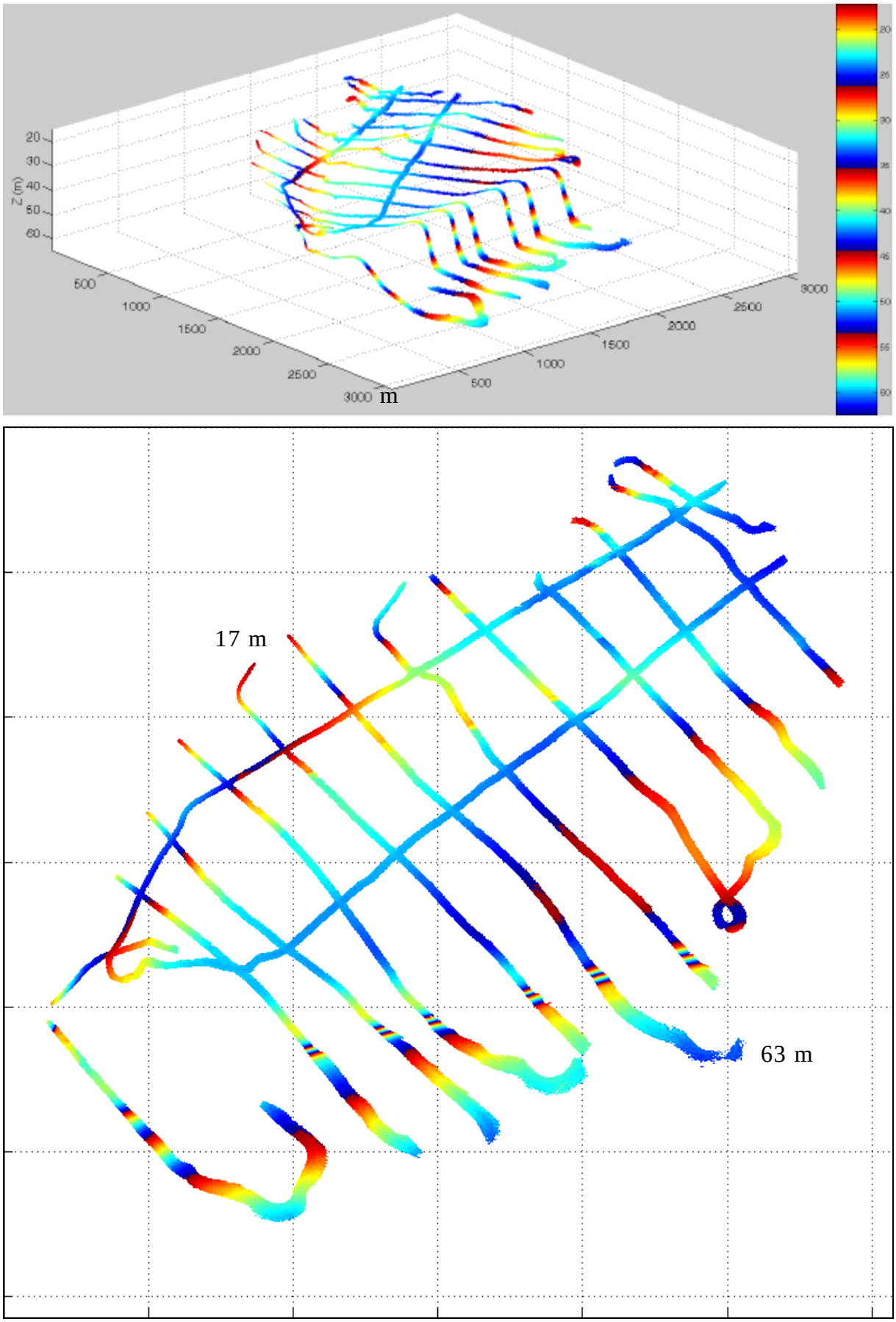


Figure 2.11 : Blanes area – the colormap is 5 times folded, from 17 m to 63 m

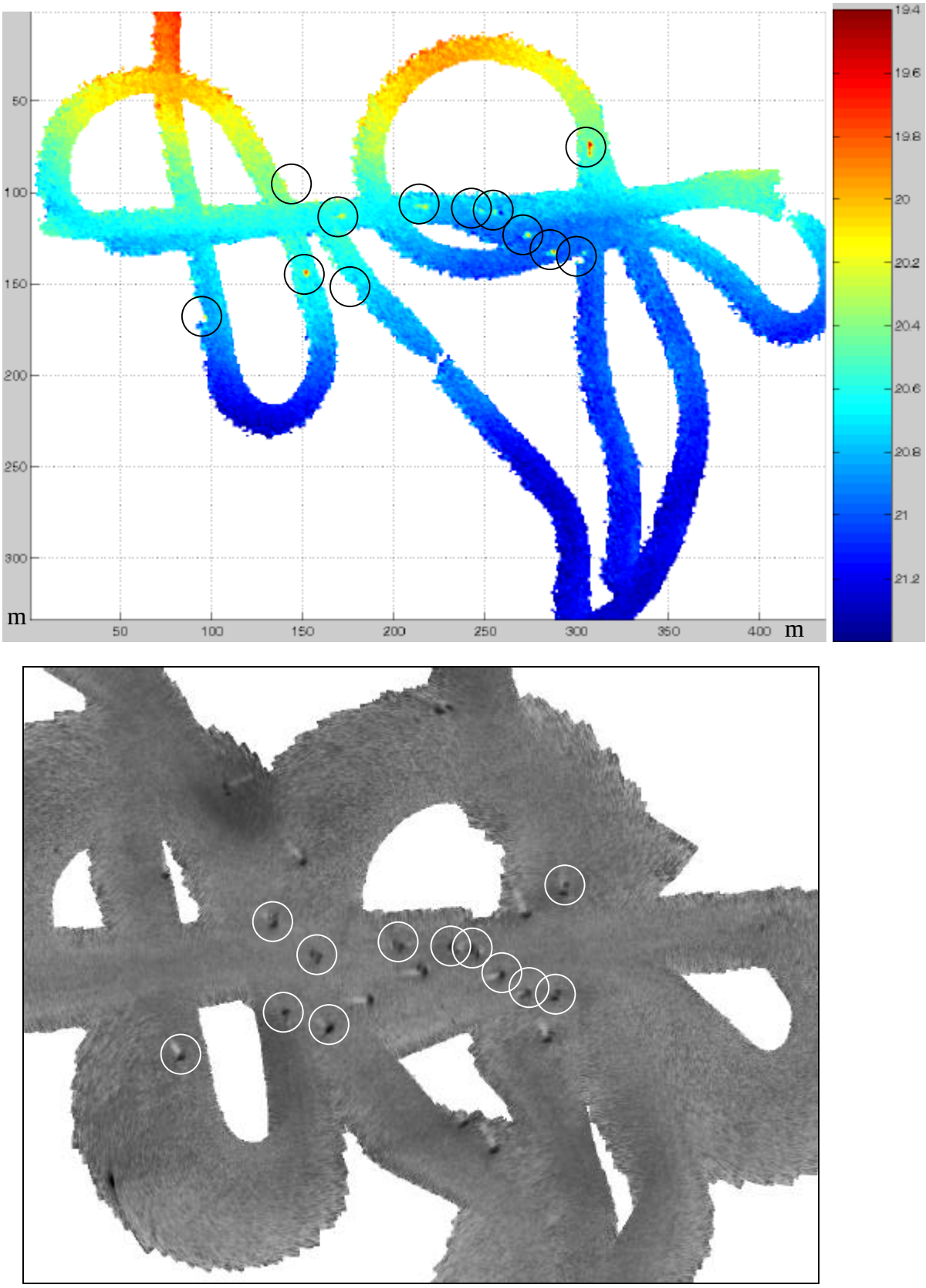


Figure 2.12 : Part of Vilanova area – Artificial reefs
Bathymetry (upper part)
Backscatter image (lower part)

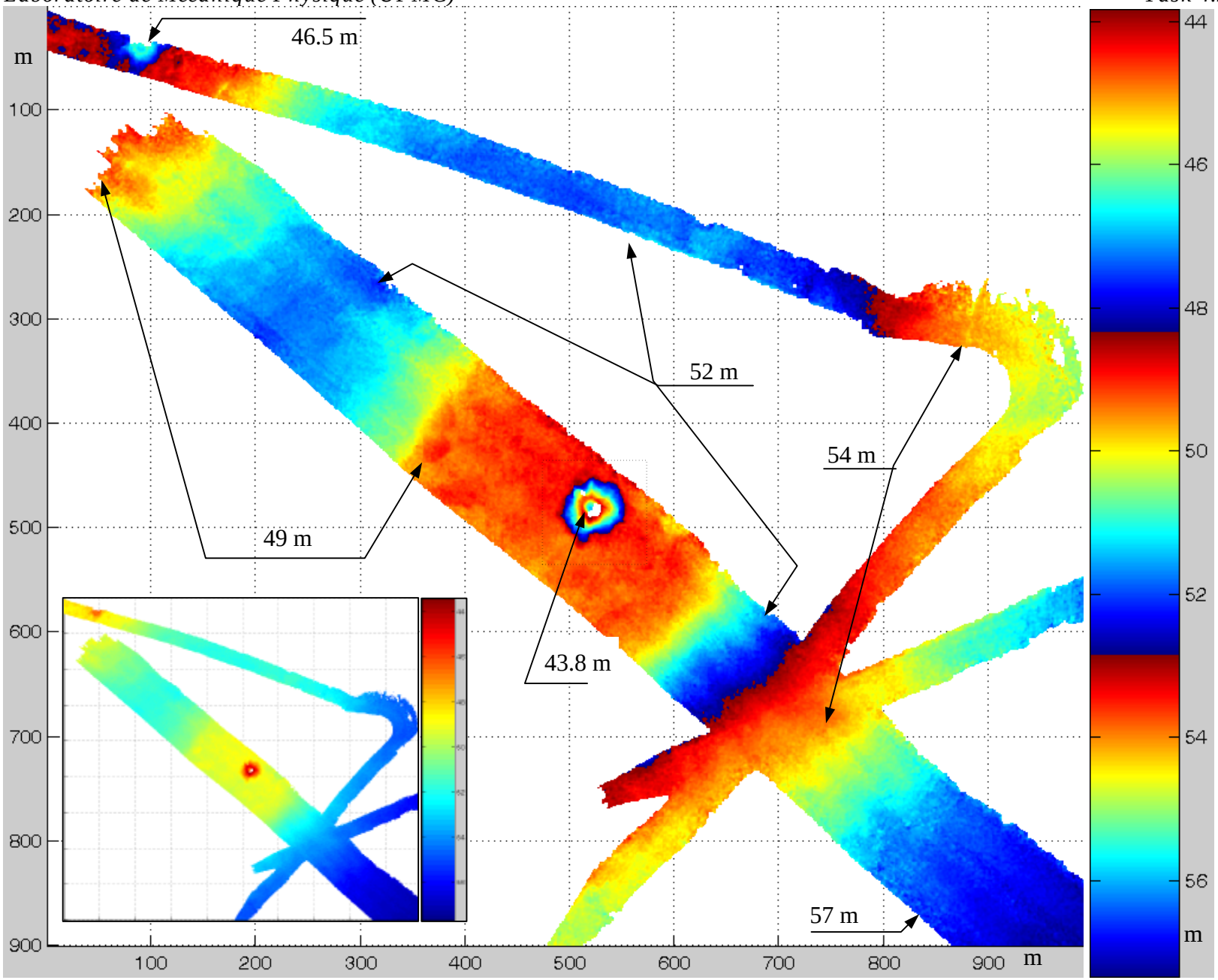


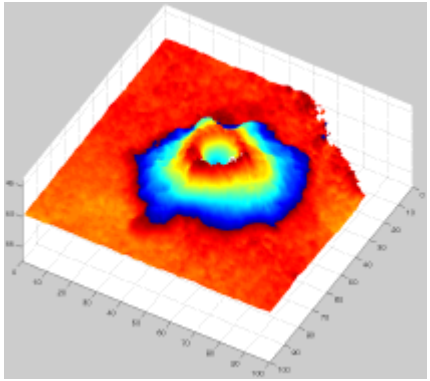

Figure 2.13 : Part of Besos

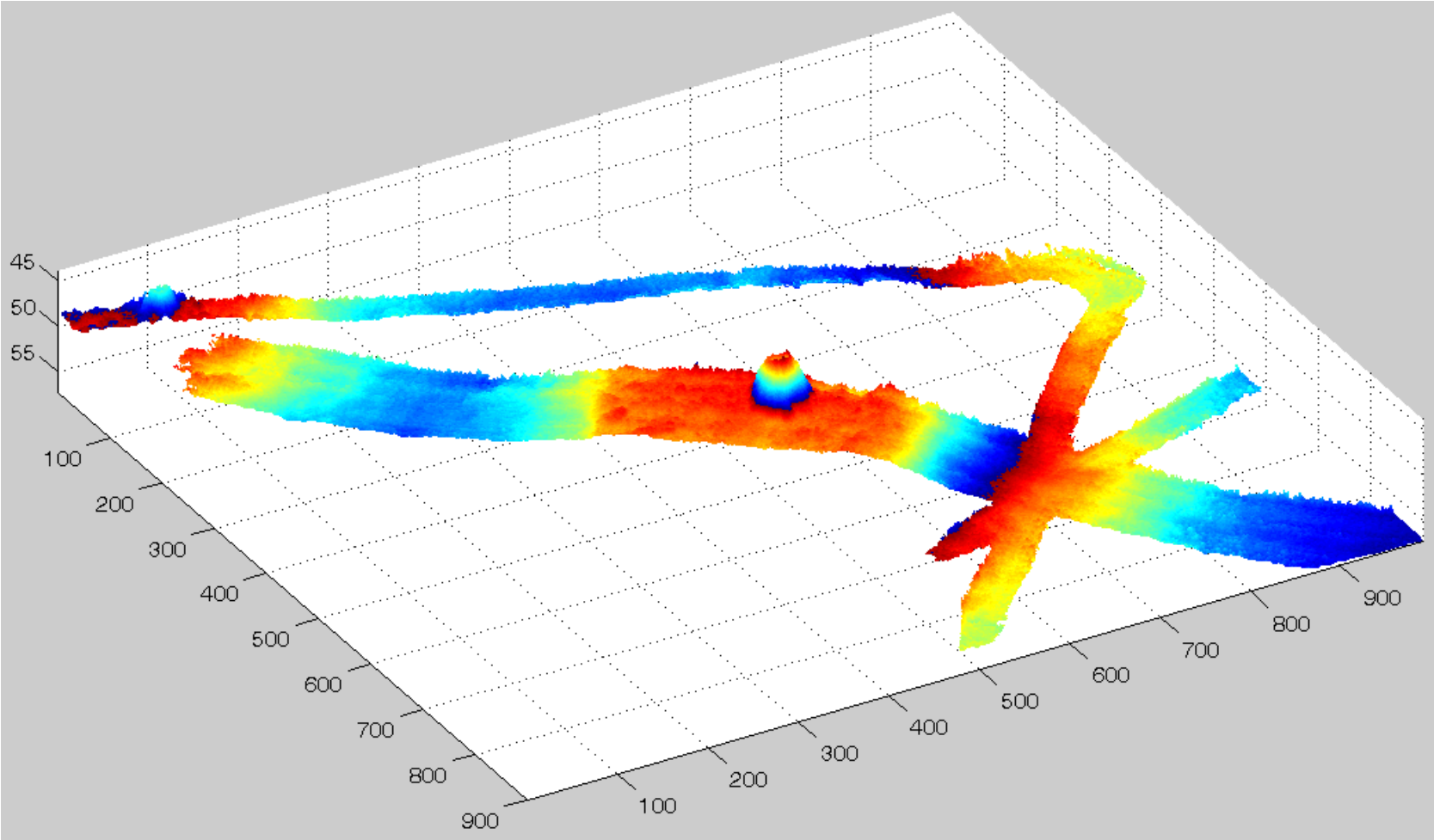


Figure 2.14 : Part of Besos area – same colormap as Figure 2.13.

## 2.7 CONCLUSION

The correction for bias described in Section 2.5.3 is based on the tuning of the lookup table between differential phase and geometric angle. An important problem remains pending in the estimate of the biases. No definite clue has been found on the best choice of the additional condition needed to solve (5.8). Specifically, assigning any reasonable small value to $b_0$ leads to the same resulting deviations after iteration. This is not a surprise : in the extreme case of a perfectly flat bottom, the chosen solution, although not unique and as far as the biases remain small, leads to a correction that cancels almost exactly the biases. A noticeable dependency of the deviations can be expected only if the relief is very tortuous and the resolution of the system very high. Additional investigations are still required to study this problem.

The calibration obtained with COSMOS may be not absolute but is quite sufficient to reduce the variance in the interferometric measurements. It can be also noticed that once the system is calibrated, a simpler algorithm can be used in operational conditions to compensate for residual biases : the lookup table is not further updated, but each mosaic layer is straightforwardly adjusted with (5.15) before merging.

At the present time, it can be stated that the performance of COSMOS to produce bathymetry with its interferometer is definitively better than what a sidescan sonar system would deliver with the equivalent interferometer. This statement is attested by Figures 2.8b and 2.10b : The deviation with a sidescan sonar would be commensurate to the average value ($\approx 0.6\%$) observed in the useful range of angles of view. The accuracy of the digital terrain models obtained with COSMOS is improved by the square root of the number of layers that contribute to build the final soundings. In the central part of the surveyed strip, this factor can rise up to about 5.

Although no simulation of in-line computation for bathymetry has been done, it has been observed that the time needed to process one ping in building ".xyz" files (Section 2.3.3) is shorter than the equivalent acquisition time. The post-processing duration required to build mosaic images is shorter either. It justifies our confidence in the feasibility to implement the in-line preview of the relief with a COSMOS-like system.

# ANNEXES

## 1. DATA POSITIONING

The problem addressed here is to find the location of the origin of the incoming echoes. Input parameters are : Mounting angles, heading, attitude (pitch and roll), heave (not addressed in this text), beam angle. To derive bathymetry, the interferometric angle and the round-trip delay are also provided. Otherwise, for imaging with the flat bottom assumption, the depth and slant range are given.

### 1.1 NOTATIONS

- $p$ Pitch
- $r$ Roll
- $h$ Heading
- $l$ Orientation of the receiving arrays in the deck plane
- $\mu$ Slant of the mounting angle : Boresight versus the deck plane
- $b$ Beam angle
- $y$ Interferometric angle
- $z$, $s$ Depth, Slant range

### 1.2 FIXED COORDINATE SYSTEM

The Fixed Coordinate System (FCS) is referenced with the unit vectors ($\mathbf{f_x}$, $\mathbf{f_y}$, $\mathbf{f_z}$), that point respectively toward North, East, and downward.

### 1.3 SHIP COORDINATE SYSTEM

The Ship Coordinate System (SCS) is referenced with the unit vectors ($\mathbf{s_x}$, $\mathbf{s_y}$, $\mathbf{s_z}$). The deck plane is defined by ($\mathbf{s_x}$, $\mathbf{s_y}$) :

- $\mathbf{s_x}$ points toward the bow ;
- $\mathbf{s_y}$ points towards starboard ;
- $\mathbf{s_z}$ is perpendicular to the deck plane, and points downward.

True heading ($h$) is taken into account by a rotation of the SCS in the horizontal plane ($\mathbf{f_x}$, $\mathbf{f_y}$). Because one follows the same convention as for angles delivered by compasses, heading is counted positively clockwise. Actually, heading is the angle that the vertical plane containing $\mathbf{s_x}$ makes with North. Specifically, $\mathbf{s_x}$ lies in the vertical plane ($\mathbf{f_x}$, $\mathbf{f_z}$) when the heading is null ($h$ = 0). The matrix $\mathbf{T_0}$ accounts for the rotation caused by heading :

$$\mathbf{T}_0 = \begin{bmatrix} \cos h & -\sin h & 0 \\ \sin h & \cos h & 0 \\ 0 & 0 & 1 \end{bmatrix} \tag{I.1}$$

Because attitude angles are obtained with a Vertical Reference Unit, pitch ($p$) and roll ($r$) are the angles that $\mathbf{s_x}$ and $\mathbf{s_y}$ make respectively with the horizontal plane ($\mathbf{f_x}$, $\mathbf{f_y}$). Pitch is positive when the bow is slanted upward, and roll is positive when starboard dives (Figure 1.1). With a null heading, the coordinates of a point of the ship are transformed from the SCS to the FCS with :

$$\mathbf{T}_1 = \begin{bmatrix} \cos p & \sin r \tan p & \tan p\sqrt{1-\sin^2 p-\sin^2 r} \\ 0 & \dfrac{\sqrt{1-\sin^2 p-\sin^2 r}}{\cos p} & -\dfrac{\sin r}{\cos p} \\ -\sin p & \sin r & \sqrt{1-\sin^2 p-\sin^2 r} \end{bmatrix} \tag{I.2}$$

Hence, the complete transform from the SCS to the FCS is derived with the product $\mathbf{T_0T_1}$.

Note that whenever pitch and roll are both not null, the projections of $\mathbf{s_x}$ and $\mathbf{s_y}$ in the horizontal plane ($\mathbf{f_x}$, $\mathbf{f_y}$) do not make an exact right angle.

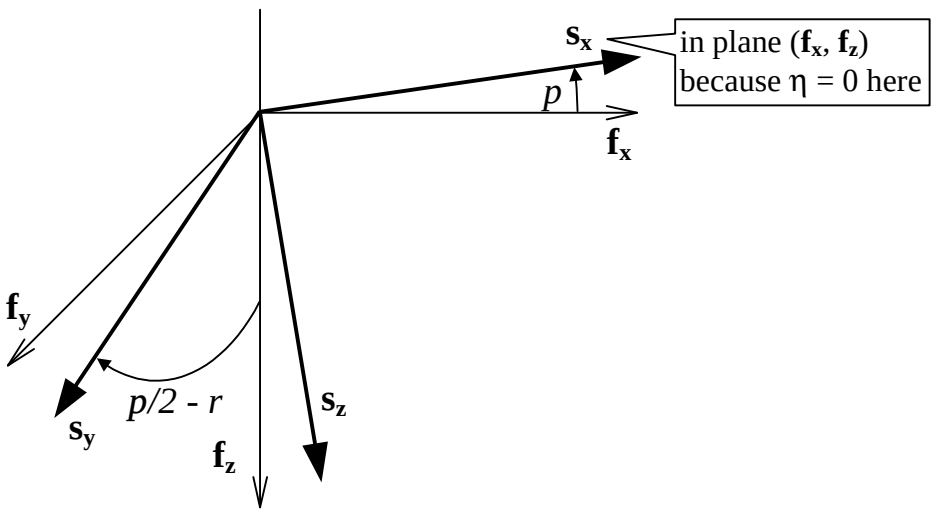


Figure 1.1 : Ship (SCS) versus Fixed (FCS) Coordinate Systems (null heading)

## 1.4 ARRAY COORDINATE SYSTEM

The Array Coordinate System (ACS) is attached to the receiving antennae. The SCS and the ACS are statically tied together through mounting angles. The ACS is introduced because beam and interferometric angles refer to this system. The ACS is given with the unit vectors ($\mathbf{a_x}$, $\mathbf{a_y}$, $\mathbf{a_z}$) : (see Figure 1.2)

- $\mathbf{a_x}$ points to boresight, i.e. the direction which is normal to the active face of the arrays ;
- $\mathbf{a_y}$ is parallel to the linear arrays and points to starboard ;
- $\mathbf{a_z} = \mathbf{a_x} \wedge \mathbf{a_y}$.

The mounting angle, $\mu$, is the angle that $\mathbf{a_x}$ makes with the deck plane ($\mathbf{s_x}$, $\mathbf{s_y}$). Following the same convention as for the pitch angle, $\mu$ is negative because the active face is slanted downward.

The receiving linear arrays ($\mathbf{a_y}$) are assumed to belong to the deck plane. The offset angle $l$ accounts for a rotation of the ACS around $\mathbf{s_z}$. The convention of sign is the same as for heading.

Coordinates in the ACS are computed in the SCS through the transform defined by :

$$\mathbf{T}_2 = \begin{bmatrix} \cos m \cos l & -\sin l & \sin m \cos l \\ \cos m \sin l & \cos l & \sin m \sin l \\ -\sin m & 0 & \cos m \end{bmatrix} \tag{I.3}$$

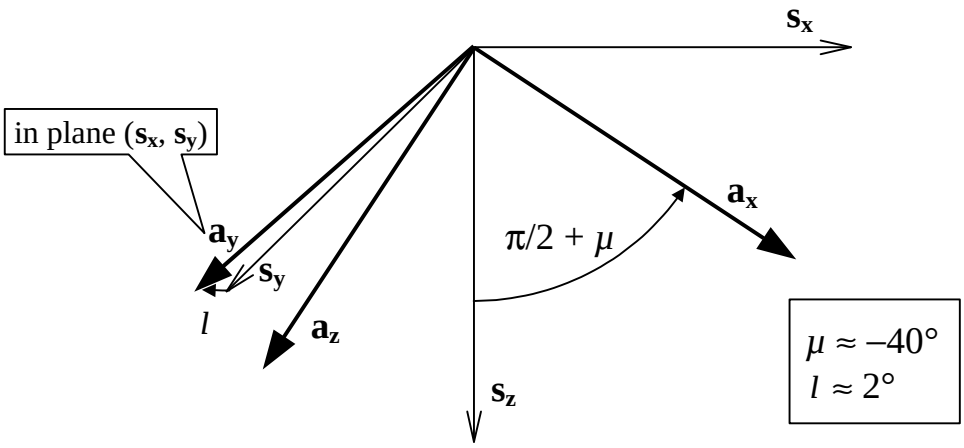


Figure 1.2 : Array (ACS) versus Ship (SCS) Coordinates Systems

Note that with a sidescan system, $l$ is close to $\pm\pi/2$ (sign "+" for the starboard mounted antennae). With a forward looking system, the angle $l$ accounts for an offset in the mechanical setup, and is very small (Figure 1.2). In the Barcelona sea trial, the mounting angles are estimated by : $\mu \approx -38.75°$ and $l \approx 1.75°$.

# 2. RAY TRACING

## 2.1 INTRODUCTION

Ray tracing is a classical problem in underwater acoustics. We consider that the celerity depends only on depth $z$. Given an initial incidence angle $0 \le q_0 < \pi/2$ at the origin $(x_0, z_0)$, and the time of flight $t$, the typical problem consists of finding the location $(x, z)$ and the incidence angle $q$ at the end of the ray.

An accurate model can be achieved in considering layers with constant gradients. Typically, one consider a set of $n$ layers whose $n$+1 boundaries are defined by the couples $(z_i, c_i)_{i = 0,\ldots,n}$, $z_i < z_{i+1}$. Within each layer ($z_i \le z \le z_{i+1}$), there is :

$$c = c_i + b_i(z - z_i) \text{ with } b_i = \frac{c_{i+1} - c_i}{z_{i+1} - z_i} \quad (i = 0,\ldots,n - 1) \tag{II.1}$$

Additional conditions usually apply at the boundaries of the stack of layers. Here, the medium $z > z_n$ is considered to be semi-infinite, with a constant positive gradient, $b_n \ge 0$. The following notations are used in the remaining part of this section : $e << 1$ is the required relative accuracy, and $s_0 = \sin q_0 / c_0$ ($s_0 \ge 0$, $c_0 > 0$).

Within a layer whose celerity gradient is a constant, rays are arcs of circle. Assuming that there is no turning point, the time of flight $\Delta t_i = t_{i+1} - t_i$ between depths $z_i$ and $z_{i+1}$ is given by :

$$\Delta t_i = \frac{1}{b_i}\ln\left(\frac{c_{i+1}}{c_i}\frac{1+\cos q_i}{1+\cos q_{i+1}}\right) = \frac{1}{b_i}\ln\left(\frac{\tan(q_{i+1}/2)}{\tan(q_i/2)}\right) = \frac{1}{b_i}\ln\left(1 + b_i\left(z_{i+1} - z_i\right)S\right) \tag{II.2}$$

with

$$S = \frac{c_{i+1} + c_i + c_{i+1}\cos q_i - c_i \cos q_{i+1}}{c_i c_{i+1}\left(\cos q_i + \cos q_{i+1}\right)} \tag{II.3}$$

When the celerity gradient $b_i$ vanishes, (II.2) is prone to a singularity that must be specifically addressed. Looking for computationally efficient formulae, we provide here consistent approximations. Any particular ray tracing algorithm can be implemented in combining the solutions of the three following elementary problems that involve a single iso-gradient layer ($b_i$), with an initial incidence angle $0 \le \theta_i < \pi/2$ ($0 \le \sin \theta_i = s_0 c_i < 1$).

Note that the solutions involving an initial angle such that $\theta_i > \pi/2$ are not explicitly given here. Problems involving reflections, at the upper or lower boundaries, are not addressed either.

## 2.2 PROBLEM #1

One looks for the horizontal displacement and for the time of flight when crossing from $z_i$ to $z_{i+1}$. By hypothesis, there is no turning point, i.e. :

$$s_0 c_i \ (= \sin\theta_i) < 1 \quad \text{and} \quad s_0 c_{i+1} \ (= \sin\theta_{i+1}) < 1 \tag{II.4}$$

There is always :

$$\boxed{x_{i+1} - x_i = (z_{i+1} - z_i)\frac{s_0(c_i + c_{i+1})}{\cos q_i + \cos q_{i+1}}} \tag{II.5}$$

If $\boxed{\tfrac{1}{2}\left|(c_{i+1} - c_i)S\right| < e}$ $S$ given by (II.3) (II.6)

then $\boxed{\Delta t_i \approx (z_{i+1} - z_i)S}$ (approximate) (II.7)

else $\boxed{\Delta t_i = \frac{1}{b_i}\ln\left(\frac{c_{i+1}}{c_i}\frac{1+\cos q_i}{1+\cos q_{i+1}}\right)}$ (exact) (II.8)

## 2.3 PROBLEM #2

There is a turning point between $z_i$ and $z_{i+1}$. One looks for the coordinates of the turning point ($x_r$, $z_r$) with $z_i < z_r \le z_{i+1}$, and for the time of flight $\Delta t_i' = t_r - t_i$ to reach this point.

By hypothesis, $b_i > 0$ and : $s_0 c_i < 1$ and $s_0 c_{i+1} \ge 1$ (II.9)

The celerity at the turning point ($q_r = \pi/2$) is $c_r = 1/s_0$. Its coordinates are :

$$\boxed{\begin{aligned} x_r &= x_i + \frac{\cos q_i}{s_0 b_i} \\ z_r &= z_i + \frac{1 - s_0 c_i}{s_0 b_i} = \frac{z_i(s_0 c_{i+1} - 1) + z_{i+1}(1 - s_0 c_i)}{s_0(c_{i+1} - c_i)} \end{aligned}} \tag{II.10}$$

The rigorous condition to be met for expressing with a development the time of flight between depths $z_i$ and $z_r$ is : $\left|1 - s_0 c_i + \cos q_i\right| < 2\left|s_0 c_i\right| e$ . However, because $\varepsilon << 1$, this condition can be reduced to $\cos q_i < 2e$ , so that finally :

If $\boxed{p/2 - 2e < q_i \le p/2}$ (II.11)

then $\boxed{\Delta t_i' \approx \frac{1 + \cos q_i - s_0 c_i}{s_0 c_i b_i} \approx \frac{\cos q_i}{b_i}}$ (approximate) (II.12)

else $\boxed{\Delta t_i' = \frac{1}{b_i}\ln\frac{1+\cos q_i}{s_0 c_i}}$ (exact) (II.13)

also $\left(\Delta t_i' = \frac{1}{2b_i}\ln\frac{1+\cos q_i}{1-\cos q_i} = -\frac{1}{b_i}\ln\left(\tan(q_i/2)\right)\right)$

## 2.4 PROBLEM #3

The time of flight, $\Delta t$, is given. After checking that the whole arc belongs to the same layer, one looks for the incidence $q$ and the displacements ($x$ - $x_i$, $z$ - $z_i$) at the end of the ray.

This problem is consistent only if the solution lies within the given layer. Let us consider first that the condition for crossing the layer exists :

$$\boxed{i < n \quad \text{and} \quad s_0 c_{i+1} < 1} \tag{II.14}$$

The given time of flight is larger than the crossing time if :

$$\boxed{\Delta t > \Delta t_i}. \tag{II.15}$$

where $\Delta t_i$ is given by (II.6), and (II.7) or (II.8). Hence, whenever (II.14) and (II.15) are both true, Pb.3 can be only considered again after propagating the ray to depth $z_{i+1}$, where : (see Pb.1)

- the abscissa of the new starting point, at depth $z_{i+1}$, is given by (II.5) ;
- the remaining time of flight is $\Delta t - \Delta t_i$.

Let us consider now that (II.14) is not true (so that there is necessarily $b_i > 0$), or that the medium is semi-infinite (last interface) with a positive celerity gradient, i.e. :

$$\boxed{s_0 c_{i+1} \geq 1 \quad \text{or} \quad \left(i = n \quad \text{and} \quad b_{i=n} > 0\right)} \tag{II.16}$$

If the time of flight is large enough so that :

$$\boxed{\Delta t \geq 2\Delta t_i'}, \tag{II.17}$$

the ray encounters a turning point ($x_r$, $z_r$), and crosses back the initial plane, at time $2\Delta t_i'$, through the point $\left(x_i', z_i'\right)$ defined by :

$$\boxed{\begin{aligned} x_i' &= 2x_r - x_i = x_i + 2\frac{\cos q_i}{s_0 b_i} \\ z_i' &= z_i \end{aligned}}. \tag{II.18}$$

Hence, whenever both conditions (II.16) and (II.17) are true, Pb3 must be addressed again with the following parameters :

- the new starting point is given by (II.18) ;
- the ray is running toward $z > z_i$ with the initial incidence $\theta_i' = \pi - \theta_i$ ;
- the remaining time of flight is $\Delta t - 2\Delta t_i'$. ($\Delta t_i'$ given exactly by (II.13)).

Let us consider now all the other cases, i.e. :

- delay ($\Delta t$) shorter than time to cross the layer (no turning point), or
- turning point exists but delay shorter than time to exit upward from layer through the entry plane.

which summarizes into :

$$\boxed{\begin{array}{l}\left(i<n \quad \text{and} \quad s_0 c_{i+1}<1 \quad \text{and} \quad \Delta t \le \Delta t_i\right), \\ \text{or} \\ \left(\left(\left(i<n \quad \text{and} \quad s_0 c_{i+1} \ge 1\right) \quad \text{or} \quad i=n\left(b_n \ge 0\right)\right) \quad \text{and} \quad \Delta t < 2\Delta t_i'\right)\end{array}} \tag{II.19}$$

<u>Note</u> : From a practical point of view, condition $\Delta t < 2\Delta t_i'$ reads also :

$$\left(1-\cos q_i\right) e^{b_i \Delta t} < 1+\cos q_i \,. \tag{II.20}$$

The celerity at the end of ray is given by :

$$\boxed{c = c_i \frac{2e^{b_i \Delta t}}{1+\cos q_i + \left(1-\cos q_i\right) e^{2b_i \Delta t}}}, \tag{II.21}$$

and the final incidence angle reads :

$$\boxed{\begin{array}{l}\sin q = \dfrac{2 s_0 c_i e^{b_i \Delta t}}{1+\cos q_i + \left(1-\cos q_i\right) e^{2b_i \Delta t}} \\ \cos q = \dfrac{1+\cos q_i - \left(1-\cos q_i\right) e^{2b_i \Delta t}}{1+\cos q_i + \left(1-\cos q_i\right) e^{2b_i \Delta t}}\end{array}} \tag{II.22}$$

if $\boxed{\left|b_i\right| \Delta t < 2e}$ (II.23)

then
$$\boxed{\begin{array}{l} x - x_i \approx s_0 c_i^2 \Delta t \dfrac{e^{b_i \Delta t}+1}{1+\cos q_i + \left(1-\cos q_i\right) e^{2b_i \Delta t}} \\ z - z_i \approx c_i \Delta t \dfrac{1+\cos q_i - \left(1-\cos q_i\right) e^{b_i \Delta t}}{1+\cos q_i + \left(1-\cos q_i\right) e^{2b_i \Delta t}}\end{array}} \quad \text{(approximate)} \tag{II.24}$$

else
$$\boxed{\begin{array}{l} x - x_i = s_0 c_i^2 \dfrac{e^{b_i \Delta t}-1}{b_i} \dfrac{e^{b_i \Delta t}+1}{1+\cos q_i + \left(1-\cos q_i\right) e^{2b_i \Delta t}} \\ z - z_i = c_i \dfrac{e^{b_i \Delta t}-1}{b_i} \dfrac{1+\cos q_i - \left(1-\cos q_i\right) e^{b_i \Delta t}}{1+\cos q_i + \left(1-\cos q_i\right) e^{2b_i \Delta t}}\end{array}} \quad \text{(exact)} \tag{II.25}$$

It can be noticed that the same expressions – given by Eqs. (II.21) to (II.25) – apply, whether the end of ray occurs before or after a turning point.

# 3. MAP MANAGEMENT

Mapping a survey can be a very memory consuming task. The total number of pixels can be large, depending on the size of the resolution cell compared to the dimension of the survey. In addition, several layers of information are involved if multiple mosaics are required, which is the case with COSMOS. Multiple images of the backscatter index can be built, each mosaic corresponding to a given range of incidence angle. Concerning bathymetry, several models of the relief can be built, each layer corresponding to a given range of interferometric angles. Moreover, several types of information have to be jointly mapped to build a single mosaic layer. Imaging requires two parameters : backscatter strengths and weighting factors. Bathymetry requires an additional intermediate weight factor. Several commercial mapping survey tools embed the capability to handle large maps. Usual research processing tools do not, at least efficiently. Consequently, we had to build our own mapping management tool.

The basic principle of the map management is to keep alive in the central memory of the computer only a small part of the survey. Let us define first a square map unit that contains $u\_side^2$ pixels. The complete survey is a 2-D collection of such map units. The active window S is also a square, made of $nb\_u^2$ map units : This window must be large enough to hold at least a complete ping plus an additional margin. Actually, a mapped ping must fit within a square surface smaller than $(nb\_u - 1)^2$ map units. Beyond the initialization step, the boundaries of a new ping are checked with respect to the boundaries of the active window. If the new ping does not fit, the active window is shifted horizontally and/or vertically as needed, the unit increment being the map unit side. In this process, map units that leave the active window are saved on disk (if flagged as containing data). On the other hand, the files corresponding to the new map units that the active window overlaps are loaded (if they exist). Doing so, the size of the survey is only limited by the amount of available mass storage.

From a practical point of view, a good balance of the parameters *u_side* and *nb_u* must be found. Given a constant maximal ping size, i.e. a constant product $p = (nb\_u - 1)\ u\_side$, the size of the window S equals : $s = p^2(1+(nb\_u - 1)^{-1})^2$. Hence, the size $s$ decreases but the disk swap activity increases as *nb_u* increases... We choose $u\_side = 128$ and $nb\_u = 8$.

The mosaicking process is based on the sequential mapping of successive pings. For this purpose, another dynamic memory space, P, whose size is identical to the active window S, is also reserved. The content of P is reset before loading a new ping. The information to be processed in this ping is then interpolated and mapped into P : The input data are structured as 2-D beam × time arrays ; Each sample is assigned the closest pixel in the cartesian grid P ; The remaining gaps between adjacent time and beam samples are then filled by interpolation. After that, the content of P is stacked in the survey window S. The process iterates with the next ping.

# 4. RELATION BETWEEN PHASE AND DELAY

## 4.1 BASE-BAND DEMODULATION

Let us consider a real signal $E(t)$ whose bandwidth $2\pi B = w_{max} - w_{min}$ ($w_{min} > 0$, $w_{max} < 2w_0$) is centered around the pulsation $w_0$. $E(t)$ can be written in term of its analytical signal $M(t)$ :

$$E(t) = \mathrm{Re}\left\{M(t)e^{jw_0 t}\right\} \tag{IV.1}$$

where $M(t)$ is a complex analytical signal of bandwidth $B$ centered at the origin.

Two delayed replica of $E(t)$ reads :

$$E_1(t) = E(t) \quad \text{and} \quad E_2(t) = E(t-t) = \mathrm{Re}\left\{M(t-t)e^{-jj}e^{jw_0 t}\right\} \quad \text{with} \quad \boxed{j = w_0 t} \tag{IV.2}$$

Within a 2-D geometry and considering that a pair of point-like receivers of an interferometer is immersed in the far-field of a point source (plane wave), the following classical relations applies :

$$j = w_0 t = k_0 d \sin y \quad \left(k_0 = w_0/c\right) \quad \text{and} \quad ct = d \sin y \tag{IV.3}$$

$d$ is the size of the baseline, $l_0$ is the wavelength corresponding to the pulsation $w_0$ with a celerity $c$, and $y$ is the geometric incident angle. The convention of sign is such that $y > 0$ when Point 1 is hit before Point 2, i.e. $E_1(t)$ precedes $E_2(t)$.

Synchronous detection is achieved by performing :

$$D(t) \equiv \left\{E(t)e^{-w_0 t}\right\}_{\text{Lowpass}} \tag{IV.4}$$

where the lowpass filter is meant to remove any spectral component outside the band $]-w_0, w_0[$, and particularly the contribution $M^*(t)e^{-2jw_0 t}$ that results from the demodulation process. Signals $E_1(t)$ and $E_2(t)$ become :

$$D_1(t) = M(t) \quad \text{and} \quad D_2(t) = M(t-t)e^{-jj} \tag{IV.5}$$

## 4.2 AM SIGNAL

The differential phase between signals $D_1(t)$ and $D_2(t)$ is then :

$$\Delta j_D = \arg\left(D_1(t)D_2^*(t)\right) = j + \arg\left(M(t)M^*(t-t)\right) \tag{IV.6}$$

Let us consider a pure Amplitude Modulated signal E(t), i.e. the phase of $M(t)$ is a constant :

$$M(t) = R(t) \quad \text{with} \quad \mathrm{d}\left(\arg\left(R(t)\right)\right)/\mathrm{d}t = 0 \tag{IV.7}$$

Hence, because $\arg\left(R(t)R^*(t-t)\right) = 0$, the differential phase of base-banded delayed AM signals reduces to the phase $j$, given by (IV.2) :

$$\boxed{\Delta j_D = j = w_0 t} \tag{IV.8}$$

The relation (IV.8) holds whenever the spectrum of $M$ is limited to the finite bandwidth [0, $w_0$[. However, it is clear that the differential phase measurement is meaningful only if the envelops of the delayed signals overlap sufficiently, i.e. :

$$Bt << 1. \tag{IV.9}$$

With interferometric measurements, one may consider to search for an estimate $t_e$ of the delay $t$ (e.g. maximum of the cross-correlation between $D_1$ and $D_2$), and to extract the differential phase from the argument of the cross-correlation function at this point, i.e. $\Delta j_D = \arg\left(D_1(t) D_2^*(t+t_e)\right)$.

## 4.3 LINEAR FILTER

The linear filtering (e.g. pulse compression) accounts for doing :

$$C(t) = D(t) * N^*(-t) \tag{IV.10}$$

so that the base-banded signals $D_1(t)$ and $D_2(t)$ (IV.5) turns into :

$$C_1(t) = C(t) \quad \text{and} \quad C_2(t) = e^{-jj} C(t-t) \quad \text{with} \quad C(t) = \int M(x+t) N^*(x) \mathrm{d}x \tag{IV.11}$$

When the filter is based on a perfect replica of the signal, there is :

$$M(t) = N(t), \tag{IV.12}$$

so that

$$C(t) = N(t) * N^*(-t) = \int N(x+t) N^*(x) \mathrm{d}x \tag{IV.13}$$

which induces :

$$C(t) = C^*(-t) \tag{IV.14}$$

The differential phase between signals $C_1(t)$ and $C_2(t)$ is then :

$$\Delta j_C = \arg\left(C_1(t) C_2^*(t)\right) = j \ + \arg\left(C(t) C^*(t-t)\right) \tag{IV.15}$$

The condition $\arg\left(C(t) C^*(t-t)\right) = 0$ is always true if and only if the phase of $C(t)$ is a constant. Because there is already (IV.14), it requires Im($C(t)$) = 0, i.e. :

$$\boxed{Q(t) = Q(-t)} \quad \text{with} \quad \boxed{Q(t) = \int \mathrm{Re}\left(N(x-t)\right) \mathrm{Im}\left(N(x)\right) \mathrm{d}x} \tag{IV.16}$$

Hence, whenever (IV.16) applies, the base-banded filtered signal have the following property :

$$C(t) \in \mathbb{R} \quad \text{and} \quad C(t) = C(-t), \tag{IV.17}$$

so that the same relation as (IV.8) holds :

$$\boxed{\Delta j_C = j \ = w_0 t} \tag{IV.18}$$

Functions $C$ and $N$ have similar bandwidths, so that the same remark as mentioned with (IV.9) applies also.

For example, (IV.16) is true if $N$ is symmetric, i.e. $N(t) = N(-t)$. Alternatively, (IV.16) is also met if $N$ has no phase variation : this is indeed the case with AM signals that undergo an adapted filtering after being reset to base-band.

# 5. COSMOS SIGNAL

## 5.1 CHIRP

The signal is sent by the transmitter of COSMOS is linearly frequency modulated, and tapered by a truncated Gaussian window :

$$E(t) = \mathrm{rect}(t/T)\exp\left(-a\,(2t/T)^2\right)\cos\left(\left(w_0 + \frac{p\,Bt}{T}\right)t\right), \tag{V.1}$$

with the following parameters :

$$\boxed{\begin{array}{l} n_0 = w_0/(2p) = 100\ \mathrm{kHz} \\ B = 3\ \mathrm{kHz} \\ T = 8\ \mathrm{ms} \\ a = -\ln 0.2 \end{array}}$$

The analytical function corresponding to (V.1) is symmetrical :

$$N(t) \equiv A_T(t)\exp\left(jp\,Bt^2/T\right), \tag{V.2}$$

so that (IV.16) is true, which implies (IV.17) and finally (IV.18). The signal compressed according to (IV.13) reads :

$$C(t) = \mathrm{rect}\left(\frac{t}{2T}\right)\exp\left(-\frac{(p\,Bt)^2}{8a}\left(1+\left(\frac{4a}{p\,BT}\right)^2\right)\right)\int_{-\frac{T-|t|}{2}}^{\frac{T-|t|}{2}} \exp\left(-\frac{8a}{T^2}\left(x - \frac{jp\,BTt}{8a}\right)^2\right)\mathrm{d}x\,, \tag{V.3}$$

With the COSMOS parameters, the following order of magnitude applies :

$$\left(\frac{4a}{p\,BT}\right)^2 < 10^{-2} << 1 \tag{V.4}$$

In addition, the shape of the compressed signal in the central part (where its magnitude remains significant) is mostly dictated by the first term in (V.3), i.e. the contribution of the integral is almost a constant within the useful range t << T. Hence, $C(t)$ reduces to :

$$C(t) \equiv \exp\left(-\frac{(p\,Bt)^2}{8a}\right), \tag{V.5}$$

whose duration (computed at $-n$ dB) is equal to :

$$t_{-n\ \mathrm{dB}} = 0.61\sqrt{na}/B \approx 0.26\sqrt{n}\ \mathrm{ms} << T\,. \tag{V.6}$$

The order of magnitude of the corresponding radial resolution is :

$$d\,r_{-3\ \mathrm{dB}} = \tfrac{1}{2}ct_{-3\ \mathrm{dB}} \simeq 35\ \mathrm{cm} \tag{V.7}$$

## 5.2 DOPPLER

With COSMOS, the data collection is performed around along-track. Hence, this geometry maximizes the radial speed, and consequently the potential Doppler effect.

Because of the radial speed $V_r$ of the platform, time is altered in the expression (IV.1) of the received echoes :

$$E(t) = E_0\big((1+e)t\big) \;\Rightarrow\; M(t) = N\big((1+e)t\big)\exp(jew_0 t) \quad \text{with} \quad e = 2V/c \qquad \text{(V.8)}$$

Hence, the Doppler effect alters the signal (before pulse compression) :

- the central pulsation is shifted by $\Delta\nu = e\nu_0 = ew_0/(2\pi)$;
- the duration is altered by a factor $(1+e)^{-1}$, i.e. a contraction if $e > 0$ ;
- accordingly, the bandwidth is altered by factor $(1 + e)$.

When the bandwidth of the signal is narrow, the two latter effects are negligible : The only significant effect of the Doppler is the frequency shift. A chirp signal (V.1) that meet the condition (V.4) becomes :

$$C(t) \equiv \exp\left(-2a\Delta_f^2\right)\exp\left(-\frac{\left(pB(t+\Delta t)\right)^2}{8a}\right)\exp(-j\cdots), \qquad \text{(V.9)}$$

$$\text{with} \quad \Delta_f = \Delta n/B = 2\frac{V}{c}\frac{n_0}{B} \quad \text{and} \quad \Delta t = T\Delta_f, \qquad \text{(V.10)}$$

Note that $\Delta_f$ is the frequency Doppler shift relatively to the signal bandwidth.

The comparison between (V.5) and (V.9) shows that the main effect of Doppler in the compressed signal is a time shift $\Delta t$, that translates into a range shift :

$$\Delta r = c\Delta t/2 = V_r T n_0/B, \qquad \text{(V.11)}$$

The survey speed with the COSMOS system is a few knots, so that :

$$V_r \le 1 \text{ m/s} \quad (e = 2V_r/c \le 0.003) \qquad \text{(V.12)}$$

It is not necessary to perform the correction dictated by (V.11) because the corresponding error in range ($\Delta r < 30$ cm) remains smaller that the radial resolution (V.7). Note that the reduction of the maximal level, $\exp\left(-2a\Delta_f^2\right)$, is also negligible.

The beamforming process can be also theoretically affected by the Doppler effect, since the frequency shift induces a shift, $\Delta b$, of the steering angle $b$ :

$$\Delta b = -e \tan b \qquad \text{(V.13)}$$

Again, this effect is negligible with COSMOS ($\Delta b < 0.04°$).